4-9285

(1)

Limpact Industries Ltd.

TITLE: High Energy Rate Compaction of Rapidly Solidified Metal Powders

Final Report
by:

R. W. Lyall, Limpact Industries Ltd.
J. D. Sullivan, Ph.D., Ontario Research Foundation
H. Shimizu, Ph.D., Ontario Research Foundation

Work on the project was conducted under the auspices of the Canada Centre for Mineral and Energy Technology, Energy, Mines and Resources Canada.

DSS File No. 15SQ.23440-4-9285
DSS Contract Serial No. 15Q84-00303
CANMET Project No.
CANMET Scientific Authority: Dr. L.E. Collins

Date: June 5, 1986

108pp

MICROMEDIA

RÉSUMÉ

Les procédés de compactage à haute énergie (HERC) sont très intéressants pour la consolidation de matières à solidification rapide (dites matières RS) parce que la surface des particules s'échauffe très rapidement pendant la consolidation , mais la chaleur engendrée est rapidement extraite à l'intérieur des particules de façon que la température de la masse de la matière n'augmente que très faiblement. L'échauffement de la surface favorise la cohésion de la poudre compactée. Un programme considérable fut mis sur pied pour l'étude des méthodes HERC, y compris le compactage par explosion et la pression mécanique à grande vitesse. L'épreuve a été faite sur des poudres de fer, des poudres de cuivre et une poudre de laiton RS pulvérisée à l'eau.

Pour les procédés HERC à faible vitesse, on a utilisé une forge mécanique PETRO-FORGE. La vitesse approximative du piston de cette presse est de 15 m/sec. La densité des échantillons compactés était élevée (théoriquement d'à peu près 93 à 96%) mais la cohésion faisait défaut. La sintérisation des échantillons n'était pas utilisable à cause de sérieuses élongations et distorsions pendant la sintérisation. Ces résultats ont été attribués aux (fortes) tensions résiduelles à l'intérieur de la matière compactée.

Pour les procédés HERC à haute vitesse, on a examiné le compactage par explosion moyennant des vitesses de combustion allant jusqu'à 5 km/sec. et ce dans le but d'établir les conditions optimales du compactage des métaux en poudre. Les paramètres étudiés pendant l'essai ont été: la vitesse de combustion, l'importance de la charge, la densité initiale de la poudre et l'effet du procédé sur les plaques mobiles et les absorbants d'énergie à l'intérieur de l'échantillon. Après examen attentif on a choisi les paramètres optimaux et on a compacté les poudres radialement. La densité des échantillons était élevée, mais leur cohésion n'était pas satisfaisante. La sintérisation des échantillons

compactés par explosion n'était pas utilisable à cause de sérieuses élongations et fendillements provoqués par de fortes tensions résiduelles. Les essais de compactage en directions linéaires ne portaient que des résultats limités.

En conclusion: le compactage par explosion des métaux en poudre ne constitue pas un procédé utilisable avant qu'un certain nombre de problèmes ne soient résolus. Ces problèmes comprennent: le manque de cohésion entre les particules, la tendance au fendillement et la présence de tensions résiduelles dans l'échantillon.

FINAL REPORT

HIGH ENERGY RATE COMPACTION OF R.S. METAL POWDERS

for

Limpact Industries Limited
Burnham Street, R.R. #4
Cobourg, Ontario K9A 4J7

Attention: Mr. Robert W. Lyall
President

J.D. SULLIVAN, PH.D.
H. SHIMIZU, PH.D.
MATERIALS DIVISION

Account No. 58-10376

29TH JANUARY, 1986.

ONTARIO RESEARCH FOUNDATION

SHERIDAN PARK RESEARCH COMMUNITY

MISSISSAUGA, ONTARIO, CANADA L5K 1B3 • (416) 822-4111 • TELEX 06-982311

WE, THE ONTARIO RESEARCH FOUNDATION, STIPULATE THAT THIS DOCUMENT IS SUBJECT TO THE FOLLOWING TERMS AND CONDITIONS:

1. ANY PROPOSAL CONTAINED HEREIN WAS PREPARED FOR THE CONSIDERATION OF THE ADDRESSEE ONLY. ITS CONTENTS MAY NOT BE USED BY NOR DISCLOSED TO ANY OTHER PARTY WITHOUT OUR PRIOR WRITTEN CONSENT.
2. ANY TESTING, INSPECTION OR INVESTIGATION PERFORMED BY US WILL BE CONDUCTED IN ACCORDANCE WITH NORMAL PROFESSIONAL STANDARDS. NEITHER WE NOR OUR EMPLOYEES SHALL BE RESPONSIBLE FOR ANY LOSS OR DAMAGE RESULTING DIRECTLY OR INDIRECTLY FROM ANY DEFAULT, ERROR OR OMISSION.
3. ANY REPORT, PROPOSAL OR QUOTATION PREPARED BY US REFERS ONLY TO THE PARTICULAR MATERIAL, INSTRUMENT OR OTHER SUBJECT REFERRED TO IN IT. NO REPRESENTATION IS MADE THAT SIMILAR ARTICLES WILL BE OF LIKE QUALITY.
4. NO REPORT ISSUED BY US SHALL BE PUBLISHED IN WHOLE OR IN PART WITHOUT OUR PRIOR WRITTEN CONSENT.
5. OUR NAME SHALL NOT BE USED IN ANY WAY IN CONNECTION WITH THE SALE, OFFER OR ADVERTISEMENT OF ANY ARTICLE, PROCESS OR SERVICE.
6. WE RESERVE THE RIGHT NOT TO COMMENCE AND/OR CONTINUE ANY WORK UNTIL PAYMENT ARRANGEMENTS SATISFACTORY TO US ARE ESTABLISHED.

TABLE OF CONTENTS

		PAGE
	SUMMARY	
1.	INTRODUCTION	1
2.	EXPLOSIVE COMPACTION PROCEDURES	3
	2.1 Powder Preparation	3
	2.2 Explosives	4
	2.3 Cylindrical Compaction	5
	2.4 Linear Compaction	9
3.	PROPERTIES OF CYLINDRICAL SAMPLES	10
	3.1 As-compacted	10
	3.2 Sintering	17
4.	PROPERTIES OF LINEAR SAMPLES	20
5.	PETRO-FORGE COMPACTION	21
	5.1 Procedure	21
	5.2 Properties of Samples	22
	5.2.1 As-compacted	22
	5.2.2 Sintering	22
6.	DISCUSSION	24
	6.1 Explosive Parameters	24
	6.2 Powder Precompaction	26
	6.3 Vacuum in Powder	28
	6.4 Central Mandrel	28
	6.5 Flyer Plate	29
	6.6 Sintering	29
	6.7 Optimum Parameters	31
7.	CONCLUSIONS	32
8.	RECOMMENDATIONS	34

APPENDICES

I Shock Waves
II Shock Waves Compaction Geometries
III Particle Surface Temperature and Compaction Rate
IV Shock Wave Pressures
V Calculating Effective Explosive Charge Sizes
VI Operation of the Petro-Forge Machine

SUMMARY

High Energy Rate Compaction (HERC) processes are attractive for the consolidation of RS materials because the particle surfaces are heated very quickly during consolidation and the heat generated is then quickly extracted into the particles resulting in only a very small temperature rise in the bulk of the material. Such surface heating would help to bond the compacted powder. An extensive program was carried out to investigate methods of HERC, including Explosive Compaction and high-speed mechanical pressing. The powders used were iron, copper, and a water atomized RS brass powder.

At the low end of HERC processes, a Petro-Forge machine was used. The ram speed of this press is approximately 15 m/sec. Samples compacted on this press were found to have a high density (approximately 93%-96% of theoretical, depending on the powder) but were not bonded. Sintering of the brass samples was not practical because of large dimensional elongations and distortions on sintering. These effects are attributed to (large) residual stresses in the compact.

At the high speed end of HERC processes, explosive compaction was investigated with explosive burn speeds up to 5 km/s to find the optimum conditions for the compaction of metal powders. The parameters included burn speed, charge size, initial powder density, and the effects of flyer plates and energy absorbers in the sample. After careful analysis, the optimum parameters were chosen, and powder samples were compacted radially. Although the samples showed high density values, they were not properly bonded. Sintering of explosively compacted samples was found to be impractical, because of large elongations, and cracking, caused by high levels of residual stress. Compaction trials using a linear geometry were of limited success.

It is concluded that explosive compaction of metal powders will not be a feasible process, unless a number of problems are solved. These problems include a lack of bonding between the particles, the tendency for cracking and the presence of high levels of residual stresses in the sample.

Final Report
Limpact Industries Limited

1. INTRODUCTION

One of the more recent developments in metals technology has been in the area of Rapid Solidification (RS). This involves processes in which a molten alloy (or element) is cooled to a solid state at a rate which is fast enough that the final system is not in an equilibrium state for that alloy. These techniques are supplementing alloying as a means of achieving superior materials structure and properties through microstructure control.

Structural alterations can include a refined grain size (including the possibility of an amorphous state), and the addition of concentrations of solutes not possible in normal equilibrium cooling. Properties of RS alloys can include increased hardness, superplasticity, improved corrosion resistance, and unique electromagnetic responses.

Since RS materials are formed using non-equilibrium processes, the products are inherently thermally unstable.

The mechanics of rapid cooling usually require that at least one dimension of the product be very small (of the order of 100μm or less). For some applications (such as transformer windings), this may not be a severe limitation, but for the production of bulk, solid components from RS materials, some type of consolidation will be required. The usual methods considered involve the procedures of powder metallurgy. These techniques invariably include a sintering stage, which can cause a deterioration in the enhanced properties of the RS alloys.

One promising method being considered for the consolidation of RS materials is shock wave compaction. A shock wave is a disturbance which passes through a sample and causes an almost instantaneous change in the pressure-volume state of the material in the vicinity of the disturbance. Shock waves are described in Appendix I of this report.

Shock wave compaction is a unique method of compacting a powder sample. It has the potential of selectively heating (and possibly melting) the outside of the powder particles [1], a feature which is desirable in the bonding of thermally unstable materials. There are, however, a number of difficulties to be overcome before this technique could become practical. If linear compaction is to be used (Shock Wave Compaction Geometries are described in Appendix II), then either large and expensive guns are necessary to accelerate a projectile, or explosives must be used, which may be a problem in industrial production. Linear compaction also requires some sort of momentum trap to capture the sample after compaction and dissipate its bulk kinetic energy. Cylindrical compaction, which must be carried out using explosives, has fewer equipment requirements, but tends to generate a structurally unsound region along the centre of the sample. Because of its simplicity and lower equipment costs, cylindrical compaction was used for most of the trials carried out in this project.

The RS material that was used for these compaction trials was a commercially available water atomized brass. To better understand the limits of this technique, iron and copper powders were also subjected to explosive compaction. In addition to using various powders, a number of other variables were examined in the compaction trials, including explosive energy density and burn speed, initial sample powder density, and the use of energy transmitters and absorbers in the sample.

This Final Report summarizes the work carried out under contract with LIMPACT. The methods used in the explosive compaction trials are described in Section 2. The properties of the cylindrical samples are analysed in detail in Section 3, and those of the linear compaction samples in Section 4. Compaction trials carried out using a high-speed mechanical press, specifically a Petro-Forge machine, are described in Section 5. An overall discussion of the various test parameters and sample properties is included in Section 6, with conclusions and recommendations in Sections 7 and 8. In addition, five appendices are attached to provide details of theories concerned with explosive phenomena.

2. EXPLOSIVE COMPACTION PROCEDURES

Two basic geometries were considered for shock wave compaction; cylindrical and linear. Shock wave propagation in these geometries is described in detail in Appendix II. Each has advantages and disadvantages and compaction trials were carried out using both geometries. The procedures are described below. Also described are the procedures involved in preparing the powders for use in the compaction samples.

2.1 Powder Preparation

The materials chosen for HERC were copper, iron and brass. One of the more important features of HERC is the expectation of particle surface heating, and possibly melting, during the passage of the shock wave (see Appendix III). Materials with a range of melting temperatures were chosen to attempt to set limits on the surface temperatures of the particles attained during compaction. These limits would be set by the evidence for melting at the surfaces of the particles with different melting temperatures.

The copper powder used was a commercial water atomized copper powder, the iron powder used was Hoeganaes 1000B water atomized iron powder, and the brass powder used was a water atomized brass with nominal composition 65% copper, 33.5% zinc and 1.5% lead.

All powders were reduced in hydrogen before being sealed into sample tubes. This was done to remove oxide layers which tend to form on fine metal powders. Such oxide layers can inhibit bonding between the powders on compaction. The reducing schedules are listed in Table I.

The powders were subjected to sieve analysis to determine their size distribution. The size distributions are listed in Table II. The brass powder used in later compaction trials (samples 9B through 21B) was pre-sieved to remove particles greater than 100 μm (150 mesh). The size distribution for this powder is also listed in Table II.

The microhardnesses of these powders are listed in Table III. Photographs of the microstructures are shown in Figure 1.

2.2 Explosives

The explosives used in this project were ANFO, Amatol and Detasheet. The important properties of the explosives are burn speed, mass density and energy density. The properties of the explosives are listed in Table IV. The procedure for calculating the effective charge size is given in Appendix V.

ANFO is a mixture of Ammonium Nitrate and Fuel Oil The mixture in these tests had 9% Fuel Oil. This is a low density, relatively slow burning explosive. It comes in a particulate form.

Amatol is a mixture of Ammonium Nitrate and Trinitrotoluene. This explosive is characterized by a higher density, higher energy density and faster burn speed than ANFO. It can be classed as a high explosive. It also comes in a particulate form. Most of the compaction trials used Amatol as the explosive.

Detasheet is the tradename for a high density, very fast burning high explosive. It comes in the form of sheets approximately 2 mm thick, with a surface density of 0.31 grams per square cm (2 grams per square inch). These sheets can be wrapped around the sample. Detasheet is also used as a starter for the other two types of explosive.

2.3 Cylindrical Compaction

The majority of the compaction trials made use of this geometry. The set-up is shown in Figure 2. There are a number of variables and variations in this procedure, and many of these have been examined.

The major advantage of this geometry is its simplicity. The symmetry eliminates the need for elaborate equipment to contain the sample during compaction. The explosive forces tend to be in balance, keeping the work piece in place. This is probably the best set-up for the explosive compaction of samples of large aspect ratio.

The basic configuration has a cylindrical tube containing the powder to be compacted, sealed at both ends. This tube is placed vertically inside a larger plastic or cardboard tube. The region between the two tubes is filled with the appropriate explosive. The explosive is detonated from the top. The detonation front progresses from the top of the sample to the bottom. As the burn progresses,

combustion product gases cause a rapid pressure increase which compresses the sample tube, compacting the powder. If the burn speed is fast enough, and the pressure is large enough, the pressure is imparted to the sample as a shock wave. (Shock waves are described in Appendix I.)

The tubes used to contain the powder were cut from lengths of rolled and welded mild steel 22.2 mm I.D. and 25.4 mm O.D. (7/8 inch by 1 inch). Sample tube lengths were 178 mm (7 inches) with 25 mm (1 inch) long steel plugs silver soldered into each end to seal the powder in the tube. Samples were weighed before and after filling to determine the powder mass, and the pre-compaction density was determined by dividing this mass by the known sample volume, determined from the dimensions of the sample tube.

There have been published claims that the presence of air in the original powder sample does not affect the final compact density [2]. To assess the effect of air on the compaction of metal powders, two samples of copper powder were made up; one was evacuated (CURV) and one was at one atmosphere of pressure (CUR). Both were compacted under the same conditions, with ANFO. The properties of the compacted samples are described in Sections 3 and 6.

Another variable in these tests is the initial powder density before compaction. This density was varied by pre-compacting the powder, in the sample tube, before explosive compaction. The apparatus to carry-out this pre-compaction is shown in Figure 3. The sample tubes were held in a mild steel die to prevent bulging of the tube walls. Hardened steel rams were inserted in the ends of the tube. Plastic plugs held the powder in place in this stage of the operation. The assembly was put into a slow press and the rams were forced into the tube through the appropriate distance to produce the required powder pre-compaction density. It was assumed that the density in the pre-compacted sample was uniform.

One of the problems inherent in the cylindrical geometry is that there is a tendency for the formation of a hole or channel down the symmetry axis of the compacted sample. The reason for this can be seen in Appendix V. The shock front progresses through the sample from all radial directions equally, causing the wave to converge at the centre of the sample. The result is a very high energy density which tends to disrupt the compact. Reflected waves travel to the outside of the sample, creating rarefaction waves which tend to rupture the sample. It is desirable to dissipate this energy and suppress the rarefaction waves.

One method of reducing this effect is through the use of an energy absorbing mandrel [3]. This takes the form of a solid metal bar located along the central axis of the sample (see Figure 4). The purpose of this mandrel is to absorb the converging shock energy and dissipate it in a solid body, rather than in the newly compacted powder sample. This also tends to suppress the reflected waves.

Some of the samples compacted in this project contained a tapered aluminum mandrel. The mandrel was tapered because it was anticipated that the diameter of the mandrel, relative to the diameter of the sample, would be an important variable. The diameter of the mandrel ranged from 1/4 inch to 3/4 inch. The precompaction sample diameter was one inch. Aluminum was used for the mandrel because it is a light material which is relatively easy to deform. This should make it a good shock absorber. The properties of the ends of the compacted sample were compared to determine the effects of mandrel diameter on the properties of the sample.

Another potential improvement would be realized if the shock front could be made "sharper". This was done by using a "flyer plate". The goal is to impart the explosive energy into a metal plate, allow the plate to accelerate to a high velocity, and then impact the plate onto the powder sample. In these trials, the flyer

plate took the form of a second tube located outside the sample tube, with a gap of approximately 1/16 inch between the tubes (see Figure 4). The outer tube is imploded by an explosive charge, and it impacts on the central tube, creating a sharp shock front.

There has been published evidence which indicates that tall charges of lower burn speed and lower energy density explosives are able to produce a bonded (although somewhat damaged) compact of aluminum [4]. To determine whether such a configuration could be used to compact RS brass powder, two cylindrical compactions were carried out using tall charges of ANFO. The charges were 6 inches in diameter and 14 inches tall. The powder samples were 7 inches tall. Both samples contained a central aluminum energy absorbing mandrel. One had an outer tube flyer plate (sample 17B) and one had no flyer plate (sample 18B).

The final densities and hardnesses of both samples were measured after compaction. The properties were, as previously, separated into those of the thick end (narrow end of the mandrel) and the thin end (wide end of the mandrel). The results of these measurements are shown in Tables VII and IX.

A final set of cylindrical brass samples was made up to be compacted under the optimum conditions, as determined in this study. This set was composed of three samples: 19B, 20B and 21B. The powder used in these samples was reduced in hydrogen at 425^{o}C (rather than 295^{o}C, the temperature used for the other brass samples) to ensure that the powder particle surfaces were as free from oxides as possible. Samples 20B and 21B had outer tube flyer plates, and all three had central energy absorbing aluminum mandrels. All were precompacted to 60% of theoretical density, evacuated and sealed.

Samples were compacted with Amatol, 19B and 20B using a moderate charge size, and 21B using a larger charge. Sample 19B was not recovered after compaction. The properties of samples 20B and 21B are shown in Tables VII and IX.

2.4 Linear Compaction

A small number of tests made use of this geometry. The set-up is shown in Figure 5.

In this procedure, the explosive forces are not balanced. The degree of powder containment must be adjusted so that the powder is compacted, but not shattered, by impact on the container. Satisfying these concerns requires careful design of the apparatus.

A flyer plate was used on all samples. The first configuration of the apparatus had a thick steel base, but it was found that the sample was destroyed by impact with the base. Subsequent tests used a thin (3/16 inch) aluminum base. It was found that the sample passed through the base on compaction. There was less of a tendency for the sample to shatter with this base.

The cylindrical tube which contained the powder, flyer plate and explosive was a 51 mm (2 inch) I.D. mild steel tube. This tube was attached with a hose clamp to flanges bolted to the base plate. The flyer plate was a 2 inch diameter by 1/4 inch thick mild steel disk. The flyer plate was held away from the powder with a styrofoam disk. This allowed the flyer plate to accelerate before impacting the powder.

The explosive used was Amatol, poured on a styrofoam disk, located on the flyer plate (see Figure 5). The Amatol was ignited with a single layer of Detasheet.

3. PROPERTIES OF CYLINDRICAL SAMPLES

3.1 As-compacted

A set of samples was made for cylindrical compaction. The sample properties are listed in Tables V, VI, and VII. In these tables, R is the ratio of explosive charge mass to sample tube wall mass, if no flyer plate was used, and the ratio of explosive charge mass to flyer plate mass, if a flyer plate was used. The variable R determines the amount of energy transferred from the explosive to the sample. Some of the compacted samples are shown in Figures 6, 7 and 8.

The first samples which were compacted contained copper powder. To investigate the effects of explosive burn speed, one sample was compacted with Detasheet (sample C1S) and one with ANFO (sample C2S). A central channel was seen in the sample compacted with ANFO, but not in the sample compacted with Detasheet. The absence of a central channel is taken to indicate that the compacting shock wave did not penetrate to the centre of the sample, creating a radial gradient in the compact properties.

Density measurements were made on both samples. The compacted density of C1S was approximately 90% of theoretical, and that of C2S was approximately 95%. All copper sample densities were measured by fluid displacement, using ethanol.

Interparticle bonding was poor in both samples, but worse in C1S.

There have been published claims that the presence of air in the original powder sample does not affect the final compact density [2]. To assess the effect of air in the compaction process, two samples of copper powder were made: one of which was evacuated (CURV) and one of which was at one atmosphere of pressure (CUR). Both were compacted under the same conditions, with ANFO. The final densities of the compacts were the same. Both samples had a central channel, implying that sufficient energy was deposited to cause the shock wave to penetrate to the centre of the sample. Hardness measurements showed that the samples had comparable hardnesses, with CUR having a hardness of approximately 140 VHN, and CURV approximately 130 VHN. It was concluded, on the basis of these trials, that the presence of air in the original powder samples does not noticeably affect the properties of the final compact. Most subsequent samples were not evacuated.

It was found, from sintering tests described in the next section, that samples compacted with Detasheet contained extremely high levels of residual stresses. The samples compacted with ANFO did not appear to be bonded when reasonably large explosive charges were used. As a result, it was decided to carry-out subsequent compaction trials using Amatol.

Further compaction trials were carried out to assess the effects of explosive charge size and initial powder density on the properties of the compacted samples.

After the passage of a shock wave with speed v_s through a sample of initial density ρ_o (initially at rest), the material behind the shock wave, with density ρ, is moving at a speed v_p given by

$$v_p = \left(1 - \frac{\rho_o}{\rho}\right) v_s$$

From this expression it follows that increasing the initial powder density should decrease the speed of the material behind the shock wave. This should have the effect of decreasing the size of the hole or channel down the middle of the sample since there is less bulk kinetic energy to dissipate at the centre of the sample.

Some samples were precompacted to the precompaction densities of 60% and 70% of the theoretical density. The procedures for this precompaction are described in Section 2. The copper samples in this phase of the investigation are designated 1C through 7C, the iron samples are 1I through 5I plus samples SR2 1/2 and F2, and the brass samples are 1B through 7B. Sample parameters are listed in Tables V, VI and VII.

The 21 samples in this phase of the investigation were examined to determine the final sample density and the size of the central channel. These properties are related to the initial powder density and the explosive charge size. The explosive used in all trials in this phase was Amatol. All densities are expressed as a percentage of theoretical.

The samples after compaction are shown in Figures 6 through 8. Also shown in Figure 7 is an empty sample container tube (marked EMPTY) which has been subjected to explosive compaction. This tube has been compacted to less than half of its original size with the smallest of the charge sizes used in this project, implying that even with this small charge size, the resistance offered by the sample tube is small. Figure 8 shows the components (marked (EMPTY) which make up the samples containing an energy absorbing mandrel, and an outer tube flyer plate.

The effects on sample properties caused by holding the explosive charge size constant and varying the initial density are shown in Figures 9 and 10. In Figure 9, the charge size is R=0.8, and in Figure 10, it is 3.3. With the smaller charge, the effect of increasing the initial powder density is to decrease the final compact density. This would seem to contradict common sense, since it might be expected that a partially compacted sample would require less energy to complete the compaction. Note that although the same amount of powder is contained in the sample tube, it is distributed over a shorter length of the tube in the precompacted samples. As a result, the powder may be compacted by the energy from less of the explosive charge. At the larger charge size (R=3.3), the decrease in final density with increasing initial density is still evident in the brass samples, but not in the iron or copper samples.

The effect of varying the initial density on the size of the central channel generated down the centre of the compacted sample is shown in Figures 9b and 10b. The results at R=0.8 are not conclusive, since the copper and iron samples have no channel (with the exception of a small hole in one copper sample), and the brass samples were not completely compacted. With the larger explosive charge size, the effect of the initial density on the central channel is quite pronounced. In all three materials, the diameter of the channel decreased with increasing initial density. For the brass samples, the use of an initial density of 70% was not sufficient to eliminate the central hole.

The effects on sample properties caused by holding the initial density constant and varying the explosive charge size are shown in Figures 11 and 12. In Figure 11, the initial density is 50%, in Figure 12 it is 70%. Both brass and copper were subjected to a decrease in final density with increasing explosive charge size (Figures 11a and 12a). In iron with an initial density of 50%, the

effect is much less evident, and with an initial density of 70%, the final density increases with increasing explosive charge size. An increase in final density with increasing charge size would seem to be the logical result.

In all samples, there is a tendency for the size of the central channel to increase in size as the charge size increases (Figures 11b and 12b), especially with an initial density of 50%. This may give a clue to the curious density vs charge size effect seen in the copper and brass samples. The newly compacted sample is probably subjected to disruptive after-shocks as excess explosive energy is dissipated in the sample. The size of these after-shocks would likely increase with increasing charge size. These after-shocks might damage the compacted sample and decrease its density. The presence of excessive shock waves in the sample may appear as large residual stresses in the final product.

An energy absorbing aluminum mandrel was placed along the centre of some of the samples (see Figure 3)to absorb the shock wave converging at the centre. It was expected that the diameter of this mandrel may be an important variable, so a tapered rod was used to vary the diameter along the length of the sample.

For this phase of the investigation, only brass powder was used. The samples are designated 8B through 16B in Table VII. The powder fraction larger than 150 mesh (approximately 100 μm) was removed by sieving. The size distribution for the resulting powder is given in Table II. The compacted samples are shown in Figure 8.

The next phase of the investigation involved compacting the powder at higher shock pressure, and in such a fashion that residual stresses may be reduced. The higher pressures were created by "sharpening up" the shock front, using a flyer plate. The flyer

plate, in this case, was a second steel tube placed around the sample tube (see Figure 3 of Section 2). The flyer plate tube had an I.D. of 28.5 mm and an O.D. of 31.4 mm, leaving a gap of approximately 1.5 mm between the tubes. The flyer plate impacts the samples tube on detonation, creating a very sharp shock pulse.

The properties of the as-compacted samples of interest in this phase are summarized in Table VIII. Also included are results from samples 6B, 7B and 3B, since they logically fall into this group. Table VIII also shows the (calculated) shock pressures developed in the samples during compaction. The procedure used to calculate these pressures is described in Appendix IV. It has been assumed that the measured density of the as-compacted sample is the same as the peak density as the shock wave passes through the sample. For final densities near 100%, this may not be an accurate assumption and the actual shock pressure could be higher. Notice in Table VIII that increasing the explosive size appears to decrease the shock pressure (compare samples 14B and 15B, or samples 6B, 7B and 3B). This decrease in pressure is probably an apparent result caused by the decrease in density, which is caused by after-shocks.

The final properties of samples 13B and 16B are not included in Table VIII since they were found to be empty after explosive compaction. These samples were compacted with a charge size R=8, a charge which is clearly too large.

One expected outcome from using the outer tube flyer plate was that the shock pulse should "sharpen up", and thus create a higher pressure. In Table VIII, compare the pressure in sample 6B with sample 14B or sample 3B with sample 15B to see that the flyer plate has the effect of causing approximately a 30% increase in shock pressure for a given R value.

The effect of this increase in pressure is an increase in compact density at constant R. This is shown in Figure 13. The data for samples with no outer tube are results from samples 6B, 7B and 3B, and the data with an outer tube are from samples 14B and 15B. All results (even those with an outer tube) show a tendency towards lower density as the explosive charge size is increased. This is probably the result of after-shocks disrupting the sample.

In Table VIII, the density values for the samples which had a mandrel are listed as having a thick end and a thin end. The mandrel has a tapered shape (see Figure 4) and it was expected that the relative diameter of the mandrel would have an effect on the properties of the compact. Samples marked "thick" are from the end in which the diameter of the mandrel was small, hence the brass section large. Samples marked "thin" are from the end in which the diameter was large. An examination of Table VIII shows that there is not a systematic trend in sample density as a function of mandrel diameter.

The depth of penetration of the shock wave was assessed by measuring the microhardness of the samples. The hardness was measured on the outside of all samples. In samples with a mandrel, it was measured on the face in contact with the mandrel. In samples with no mandrel, it was measured near the centre of the sample. The results of these measurements are shown in Table IX. With the exception of sample 9B, the hardness is approximately 220 VHN on the outside. On the mandrel side, the average hardness was approximately 210 VHN. Of the samples with no mandrel, in the one with R=1, the hardness at the centre was down to approximately 100 VHN and in the one with R=3, it was approximately 205 VHN at the centre. From the above observations, it is concluded that the shock pulse travelled to the depth of the mandrel in all cases, and to the centre of the

sample for the case in which R=3. The hardness of the original powder was approximately 85 VHN and thus the shock does not seem to have reached the centre of the sample for the case R=1.

The compacted powder adjacent to the mandrel had a tendency to chip and flake. This may indicate an impedance mismatch between the powder and the mandrel, making the transfer of shock pulse energy into the mandrel inefficient.

Of the two samples compacted with charges of ANFO which were twice the height of the sample itself, the one with no flyer plate was found to have a density of approximately 100% theoretical. The sample with the flyer plate had a density of 95-96% theoretical. Neither sample showed evidence of bonding.

A number of samples were mounted for metallographic examination. Portions of these samples were also subjected to post-compaction sintering. The microstructures before and after sintering are examined in detail in the next section, which deals with the effects of sintering on explosively compacted samples.

3.2 Sintering

None of the samples was properly bonded after explosive compaction. As a result, a number of the brass samples was subjected to sintering after compaction. Sintering was carried out in a hydrogen atmosphere for one half hour at a temperature of either 700°C or 870°C. 870°C represents the standard industrial sintering temperature for brass samples, and 700°C is approximately 3/4 of the melting temperature of the brass used in these trials. The properties of samples 1B through 7B are shown in Table X, and those of samples 9B through 15B are shown in Table XI, together with information concerning their dimensional stability measured before and after sintering.

An examination of Table X shows that the effect of increasing the explosive charge is an increase in the amount of dimensional change on sintering (compare samples 6B, 7B and 3B). The effect of increasing the initial density is negligible (compare samples 1B, 2B and 3B). Dimensional changes are more pronounced in samples sintered at 870°C.

These sample length changes appear to be caused by the release of internal residual stresses created by the shock wave. The length changes in the explosively compacted samples are comparable to those in the Petro-Forge compacted samples (Section 5), but they tend to be in the opposite sense (ie. explosive samples tend to shorten, Petro-Forge samples tend to elongate). This effect can be attributed to the fact that the shock pulse travels parallel to the central axis in the Petro-Forge samples and perpendicular to it in the explosive samples. The elongation occurred in the direction perpendicular to the shock wave, in both cases.

To further assess the effects of shock wave compaction and sintering, the hardness on the outside of samples 9B through 15B was measured before and after sintering. These results are also shown in Table XI. The higher sintering temperature usually (but not always) results in the lowering of the post-sintering hardness values. Since the original powder hardness is 85 VHN, it can be seen that the sintered hardness is often less than that of the original powder.

Samples of unsintered and sintered compacts were mounted for metallographic examination. This was done to attempt to determine the cause of the large dimensional changes occurring in the compacts on sintering. Only samples sintered at 870°C were examined microscopically, since they showed the largest changes on sintering. The samples studied in most detail were 12B and 15B, which had the highest density of all samples compacted without and with the central energy absorbing mandrel, respectively. The microstructures of these samples are shown in Figures 14 through 17.

In the figures showing sample 12B (Figures 14 and 15), "inside" refers to the side close to the energy absorbing mandrel. For 15B (Figures 16 and 17), "inside" refers to the region near the centre of the sample. For both samples, "outside" refers to the region near the tube wall.

The most noticeable feature of 12B was the large amount of cracking near the inside edge of the compacted sample, even before sintering (Figure 14). Sample 15B also had some cracking near the inside edge. Portions of both samples near the outside edge showed good densification before sintering. Sintering caused a considerable increase in porosity for 15B, especially near the outside edge (Figure 17). There is a less noticeable increase in porosity on sintering for 12B, but the cracking is worse after sintering (Figure 14b). All samples showed considerable macroscopic cracking, clearly visible to the unaided eye, after sintering.

Grain size measurements were made on the microstructures of samples 11B, 12B, 14B and 15B. The results are presented in Table XII. (The original powder size distribution, as determined by microscopic examination, is also reported in Table XII). The mean and standard deviation were calculated from measurements on 18 grains in each sample and from 72 measurements on the precompacted powder.

From Table XII, it can be seen that sample 12B has a grain size which is considerably smaller than that of the original powder, and sample 11B before sintering has a structure also somewhat smaller. The rest of the samples have grain sizes only very slightly smaller than that of the original powder.

Although sintering does help to bond the powders, the material is still clearly weaker than conventional brass stock.

4. PROPERTIES OF LINEAR SAMPLES

The major limitation in the use of the cylindrical geometry is that of creating a central channel in the compacted sample. This effect is caused by the converging shock waves. The channel can be eliminated by the use of a linear compaction geometry. The geometry is shown in Figure 5.

The passage of a shock wave through such a sample is described in detail in Appendix II. There are advantages and disadvantages of this geometry. With careful and proper design, after-shocks can be suppressed, eliminating the central channel. However, the passage of the shock wave through the sample causes the compacted powder to attain a velocity which could be as high as one km/sec or more. A suitable momentum trap must be used to decelerate the compact without damaging the sample.

The apparatus used in the first trials is shown in Figure 18. In this case, the compacted piece was arrested by a backing plate of 1/2 inch thick steel. The explosive was Amatol, with a charge depth of 1.5 cm. The Amatol was ignited by a layer of Detasheet. It was found that the sample was shattered after compaction and the broken pieces did not show any evidence of interparticle bonding.

Subsequent trials used backing plates of 3/16 inch thick aluminum. The sample powder was 1.0 cm deep, and explosive charge depths of 2.0 cm and 2.5 cm were used. The sample compacted with a 2.0 cm deep charge was densified, but not bonded, after compaction. The sample compacted with a 2.5 cm deep charge was shattered after compaction. Both samples were driven through the aluminum backing plate by the force of the explosion. The formation of a better momentum trap and the optimization of explosive charges may allow the compact to survive the compaction without shattering.

The properties of the disk compacted with 2.0 cm of Amatol were measured. The final density (measured by buoyancy) was 96.6%. The hardness, measured using Rockwell B and C, corresponded to 832 VHN in the centre of the top of the disk, and 410 VHN on the outside top edge. The hardness of the top as measured by Vickers hardness indentation using a 5 kg load, was 132 VHN. The reason for this discrepancy is not clear, but the material does not appear to behave plastically, as illustrated by a series of photographs shown in Figure 19. There is considerable crumbling and cracking around the indentation in the compacted sample, indicating poor bonding in this region. For comparison purposes, indentations in samples of cylindrically compacted brass, and in wrought brass, are also shown in Figure 19. There is much less crumbling in the cylindrical samples, but none of the explosively compacted samples shows the plastic deformation visible in the corners of the indentation in wrought brass.

5. PETRO-FORGE COMPACTION

5.1 Procedure

Explosive compaction is a process which takes place at the high speed end of HERC processes. To better understand the need for working at this extreme speed, tests were carried out on a Petro-Forge machine using compaction rates at the low-speed end of HERC. Ram speeds on this device are approximately 15 m/sec, much less than explosive burn speeds of approximately 5 km/sec. The operation of the Petro-Forge machine is described in Appendix VI.

A total of twelve samples was compacted on the Petro-Forge machine, four each of copper, iron, and brass. The samples were compacted in a 1 inch (2.54 cm) diameter cylindrical die. The energy of the machine was set so that the energy density on compaction was 34 Joules per gram of sample powder (compared with 200-300 Joules per gram for explosive compaction). It had been found that energy densities in excess of this amount resulted in damage to the die and problems in extracting the compacted sample. The die walls were coated with a graphite die wash to assist in removing the compact.

5.2 Properties of Samples

5.2.1 As-compacted

It was found that, although densified, the powders were not bonded. Portions of the compacts could be broken away easily by hand. Final compact densities were determined by fluid displacement, and are listed in Table XIII. The mean density of the copper samples was 93.0%, iron was 95.3% and brass was 95.6%.

The copper samples were slightly cracked after compaction. Both the iron and brass samples were smooth and uniform after compaction. There was no evidence of bonding in any of the as-compacted samples.

5.2.2 Sintering

The samples compacted on the Petro-Forge were not properly bonded, making sintering mandatory.

All sintering was carried out in a hydrogen environment for a period of one hour. Sintering temperatures, final sintered sample dimensions (relative to start dimensions) and densities are listed in Table XIV.

The copper samples exhibited a considerable amount of cracking and distortion as a result of sintering. The final compact densities after sintering were very low and the product was of poor quality.

Dimensional and density changes in the iron samples on sintering were very small at both temperatures. In general, all four iron samples seemed to be of good quality.

The brass samples sintered at 700^{o}C were well formed. Dimensional and density changes on sintering were very small. The brass samples sintered at 870^{o}C showed some cracking and slight bulging on the flat ends. The sample had changed from a yellow "brass" colour to a brownish colour. The decrease in density was rather large. The largest contribution to dimensional changes appeared to be from an increase in sample length.

The mechanical properties measured were hardness and flexural strength. The hardness of the heat treated compact was measured using the Rockwell Superficial 15% test (15 kgf and a 1/16 inch ball). This test was used because the hardness indenter did not come to a full stop during other types of hardness tests that were tried. The results of these hardness tests are listed in Table XV. Original powder hardnesses were given in Table III in Vickers Hardness Number (VHN). For comparison purposes, these results have been converted to a Rockwell Superficial 15T scale using conversion tables in ASTM E140-83. All sample hardnesses have been reduced from the original powder hardness by sintering. Both copper and brass showed an added decrease in hardness at the higher sintering temperature. The hardness of the iron sample was not noticeably further affected at the higher sintering temperature.

Flexural strength measurements were carried out on bars cut from the sintered Petro-Forge samples. The bars measured 10mm x 10mm x 32mm (3/8 inch x 3/8 inch x 1 1/4 inch) and were broken on an Instron machine in a three-point bend test, using a span of 25mm (1 inch). Two bars (designated a and b) were cut from each Petro-Forge compact tested. The flexural strength (S) was calculated from the equation [5]:

$$S = \frac{3PL}{2bd^2}\left(1 - \frac{4d}{3\pi L}\right)$$

where P is the load to fracture, L is the span, b is the sample width and d is the sample depth. Results for the brass and iron samples are listed in Table XVI. Copper samples were not tested because of their obvious poor quality. The strength of the brass was greater at the higher sintering temperature, whereas the iron seems to have reached its highest strength even at the lower sintering temperature.

6. DISCUSSION

This discussion concentrates on the following areas: the explosive parameters, the effects of vacuum on the powder samples, the effects of powder precompaction, advantages of a central energy absorbing mandrel, the advantages of a flyer plate, the effects of sintering on explosive compaction samples and an assessment of samples compacted under what are considered to be the optimum conditions as determined in this study.

6.1 Explosive Parameters

The formation of a shock wave in a porous metal sample is governed by a number of parameters. One set of parameters is associated with the explosive charge used to provide the consolidation energy.

Choosing the proper combination of parameters for the explosive compaction of a powder sample is an involved process. The burn speed of the explosive must be high enough to produce a shock wave, but not so high that it creates excessive residual stresses in the final compact. The charge size should be large enough to compact and bond the powder, but not so large that the sample is damaged by subsequent after-shocks which are reflected back through the sample. The containers of the two samples compacted with the largest explosive charge were found to be empty after compaction, indicating a charge which was much too large.

Samples compacted with ANFO, the low density, low burn speed explosive, were not bonded, even when very large charge sizes (up to a diameter of 6 inches in some cases) were used. Increasing the size of the explosive charge would require an increase in the thickness of the layer of explosive around the sample. This would be expected to decrease the sharpness of the shock wave.

It was decided to look at a higher density, faster burn speed explosive. The next explosive used was Detasheet. It was found that a small charge was enough to densify the sample, but that the material had very high levels of residual stress. This was demonstrated by the large amount of cracking seen in the compacted sample.

A compromise was made on explosive energy density and burn speed in the choice of Amatol as the explosive. Most of the compaction trials were carried out using Amatol.

Having chosen the explosive, the remaining variable was the charge size, R. The sample parameters which were monitored were the final density, and the size of the central channel, as a function of R.

The results of this stage of the investigation are shown in Figures 9 and 10 for samples containing powders at 50% and at 70% of the theoretical density of the material. Of the three materials examined, brass, copper and iron, at the initial densities of 50% and 70%, both brass and copper exhibited an apparent decrease in final density with increasing explosive charge (Figures 9a and 10a). In iron with an initial density of 50%, the effect was much less visible, and with an initial density of 70%, the final density increased with increasing explosive charge size.

In all samples, there was a tendency for the size of the central channel to increase in size as the charge size was increased (Figures 9b and 10b), especially with an initial density of 50%. This may give a clue to the curious, density vs explosive charge size, effect seen in copper and brass samples. The newly-compacted sample is subjected to disruptive after-shocks as excess explosive energy is dissipated in the sample and the size of these after-shocks increases with increasing explosive charge size. These after-shocks could damage the compacted sample and decrease its density. Excessive sample elongations on sintering demonstrated the existence of large residual stresses in the compact.

The optimum charge size is one which densifies the sample with the minimum central channel diameter and the maximum final density. For Amatol, this occurs for a charge size R between 1 and 3.

6.2 Powder Precompaction

The process of shock wave consolidation of a porous metal sample involves two processes: the compaction of the powder, and the bonding of the compacted powder particles. In the process of compaction, the sample is accelerated to a final velocity, v_p, as described in Appendix I. This velocity is dependent on the shock

wave velocity, the initial sample density and the final density. It would be desirable to reduce the final velocity of the particles and direct more of the shock energy into bonding processes, without a loss in final compact density. An examination of the equations of Appendix I shows that this can be accomplished by precompacting the powder sample. The procedures used to precompact the powder are described in Section 2.3.

The effects on sample properties caused by holding the explosive charge size constant and varying the initial density are shown in Figures 11(a) and 12(a). In Figure 11, the charge size is R=0.8, in Figure 12, it is 3.3. With the smaller charge, the effect of increasing the initial powder density is to decrease the final compact density. This would seem to contradict common sense, since it might be expected that a partially compacted sample would require less energy to complete the compaction. Note that although the same amount of powder is contained in the sample tube, it is distributed over a shorter length of the tube in the precompacted samples. As a result, the powder may be compacted by the energy from less of the explosive charge. At the larger charge size (R=3.3), the decrease in final density with increasing initial density is still evident in the brass samples, but not in the iron or copper samples.

The effect of varying the initial density on the size of the central channel generated down the centre of the compacted sample, is shown also in Figures 11(b) and 12(b). The results at R=0.8 are not conclusive, since the copper and iron samples have no channel (with the exception of a small hole in one copper sample), and the brass samples were not completely compacted. With the larger explosive charge size, the effect of the initial density on the central channel is quite pronounced. In all three materials, the diameter of the central channel decreased with increasing initial density. For the brass samples, the use of an initial density of 70% was not sufficient to eliminate the central hole.

6.3 Vacuum in Powder

There have been published claims that the presence of air in the sample powder does not affect the final compact density. To assess the effects of air in the compaction of the samples described in this report, two samples of copper powder were made up; one of which was evacuated (sample designated by CURV) and one of which was at one atmosphere of pressure (sample designated by CUR). These samples are described in Table V. The samples were compacted with ANFO under identical conditions.

Both compacted samples had central channels, indicating that the shock pulse had penetrated to the centre of the sample. Hardness measurements showed that the samples had comparable hardness, with CUR having a hardness of approximately 140 VHN and CURV approximately 130 VHN. The densities of the compacts were the same. It was concluded that the presence of air in the original powder did not affect the properties of the final compact.

With the exception of brass samples 19B and 20B and 21B, the samples compacted in this project were not evacuated.

6.4 Central Mandrel

The cylindrical compaction geometry has the disadvantage that the shock pulse converges along the central axis of the sample. This results in a high energy density in that region, and the formation of reflected pulses which tend to disrupt the compacted sample. One method of reducing the effect of the convergence of the shock pulse is to place an energy absorbing rod or mandrel along the central axis of the powder sample. This allows for the dissipation of the excess shock energy in a wrought solid rod rather than in the newly compacted powder.

It was expected that the relative diameter of the central mandrel would have an effect on the properties of the compact. Rather than having a number of samples with different mandrel diameters, conical mandrels were used, so that the diameter of the mandrel varied with position along the sample.

The mandrels used were made of aluminum because it was thought that the low yield strength and ease of deformation of this material would make an effective shock absorber. An examination of Table VII shows that there is no systematic trend in sample properties as a function of mandrel diameter.

6.5 Flyer Plate

One method of increasing the shock wave pressure without increasing the energy of the pulse is to "sharpen up" the pulse. The shockfront then is sharply defined and extends over a smaller volume of the sample. This can be done by using an intermediary projectile to carry the explosive energy to the sample. The setup is much like that used in explosive welding, in which one of the components to be joined is accelerated into the other by an explosive charge. The accelerated component is called the flyer plate, and this terminology is used here to describe the projectile used in these compactions.

As described in Section 2.3, the flyer plate used in the compaction trials on cylindrical samples was a tube located outside the sample tube. This outer tube flyer plate was imploded onto the sample tube, causing the sample to be compacted radially.

Samples with an outer tube flyer plate were made up both with and without a central aluminum energy absorbing mandrel. The properties of these samples are described in Table VII. The effect of using a flyer plate can be seen in Figure 13. This figure shows

the final density of samples compacted both with and without the flyer plate. For a given explosive charge size (R), the final densities of samples compacted with a flyer plate were larger than those with no flyer plate. The effect of the flyer plate on shock pressure can be seen in Table VIII, which shows the calculated shock wave pressure in a number of the brass samples. (See Appendix IV for a description of this calculation.) Compare sample 14B with 6B or sample 15B with 3B to see the increase in shock wave pressure caused by the flyer plate.

The theory that the shock wave pressure is increased, at constant explosive charge size, by the use of a flyer plate, would appear to be confirmed by these results.

6.6 Sintering

Since none of the explosively compacted samples was bonded, a number of them were subjected to sintering, as described in Section 3.2. These sintering trials demonstrated a number of important features of explosive compaction.

The dimensional changes in the samples on sintering were very large (often of the order of 10% or more). This level of enlargement is much greater than those in traditional P/M processing, and with the associated increase in porosity renders sintering of these types of samples impractical.

Although the strength of many of the samples was increased by sintering, it was not increased to the point of being useful in a practical application. This would seem to eliminate sintering as a means of bonding explosively compacted samples.

Microscopic examinations of samples before and after sintering showed that the dimensional changes were caused by the formation and growth of pores throughout the sample. The growth of these pores causes the bulk density of the sample to decrease.

Measurements of grain size distributions in the samples before and after sintering (Table XII) indicated that the grains did not grow significantly on sintering. The grain size distribution of the compacted samples was not significantly different from that of the measured powder size distribution of the sample powders before compaction. From this it can be suggested that the powder particles are under very high residual stress in the sample and, on relieving these stresses by sintering, the powder particles tended to return to their original shapes, creating cavities.

The sintering temperature required to cause any significant bonding in the sample is rather high (essentially, the usual industrial sintering temperature). For thermally unstable RS materials, the effects of such a heat treatment on the RS properties would be detrimental.

6.7 Optimum Parameters

The final stage of this investigation was to examine the parameters and choose the optimum value for each. The outcome of this process was a set of RS brass samples compacted under the most favourable conditions of any in this investigation.

It has been found that precompaction of the sample powder decreased the size of the central channel in the final compact, implying a decrease in the intensity of after-shocks. This final set of samples was precompacted to 60% of theoretical density. (Note that precompaction does not increase the final sample density.)

A central energy absorbing aluminum mandrel was found to eliminate the central channel, also implying the suppression of the size of after-shocks. Energy absorbing mandrels were used in this final set of samples.

The use of a flyer plate was found to sharpen up the shock pulse and increase the final density for a given explosive charge size. A flyer plate was used on two of the three samples in this set. Unfortunately, the sample with no flyer plate was not recovered after compaction, and its properties are not known.

Although a vacuum was found to have no effect on the properties of the final compact, this set of samples was evacuated. This was done on the chance that air in the sample may form an oxide layer on the powder particles during (or before) compaction.

The temperature used for the hydrogen reduction of the oxide layer on the brass powders was increased from 295^{o}C to 425^{o} to ensure that the powders in the samples were completely reduced.

In general, these samples were compacted under the most favourable conditions that could be determined from the results of this investigation. In spite of this, the properties of these samples were found to be no better than those of the best of the earlier samples.

7. CONCLUSIONS

This report describes a thorough investigation of the parameters involved in the High Energy Rate Compaction of metal powders. The conclusions of this investigation are as follows:

The use of a high speed press is not a practical method of consolidating metal powders. The compacted samples had reasonably high final densities (93-96%), but the powder particles were not bonded. Sintering caused large dimensional changes in all but the iron samples. These dimensional changes make sintering impractical with these samples.

It was not conclusive whether a vacuum in the powder sample had any effect. It did not have an effect on the final density of the samples, and none of the samples (evacuated or otherwise) were bonded.

The precompaction of the sample powder has the effect of decreasing the size of the central channel, but does not affect the final density or aid in particle bonding.

The use of a flyer plate sharpens up the shock front, effectively increasing the shock pressure for a given shock energy. This results in an increase in the final density.

The use of an energy absorbing mandrel eliminates the central channel formed by the coverging shock wave. A disadvantage of this setup is that the final sample is composed of two types of material: the densified metal powder and the mandrel. The diameter of the mandrel is not crucial, but a larger diameter (relative to the sample diameter) is probably better.

Success using the linear compaction geometry was limited, and a considerable effort will be required before this configuration produces a reasonable compact.

There was no evidence of bonding or particle surface melting in any of the samples (iron, copper or brass) although sintering of the Petro-Forge compacted iron samples did produce a bonded sample. There was, however, evidence of excessive residual stresses in the compacted samples. There was extensive cracking after compaction and this cracking was made worse by sintering.

In view of the difficulty experienced in producing a compacted sample which was bonded, a telephone conversation was initiated between ORF and Dynamic Compaction International, a California based company which carries out explosive compaction experiments on a contract research basis. DCI claims to have produced fully dense and bonded samples of METGLAS and is currently experimenting with the compaction of diamond and ceramic materials.

The methods used in this project were briefly summarized and the results described. DCI expressed the opinion that ORF's efforts were encouraging and in line with what was to be expected in the process of investigating the explosive compaction of a powder.

DCI claims that a fully dense and bonded sample can be produced using even slow burning explosives (such as ANFO) if the geometry is correct.

Every powder compacts differently, and there are many variables to investigate, such as:

- Explosive type (or types)

- shock transfer medium

- geometry
- evacuation of powder sample (still controversial, even at DCI)
- precompaction
- how to evacuate and precompact
- etc.

It is evident, from this investigation and the telephone conversation with DCI, that a significant amount of work is required before explosive compaction can be a viable commercial or industrial process for the consolidation of metal powders.

8. RECOMMENDATIONS

1. In view of the results of this investigation and the discussion with DCI, further investigations into the dynamic compaction of RS powders should concentrate on primary shapes, such as rods and plates.

2. Possible areas which could be considered (in addition to those suggested by DCI) include:

   - reduction of oxide layers on metal powders
   - improved confinement of sample powders, so that larger explosive charges can be used
   - improvements in linear compaction techniques.

3. There is considerable interest in copper nickel and copper nickel aluminum alloys and future investigations in explosive compaction should use powders of these alloys.

J.D. Sullivan, Ph.D.
Scientist
Materials Division

:lu
attach.

1. W.H. Gourdin, J. Appl. Phys. 55, 1984, pp172-181.

2. Y. Sano and K. Miyagi, Int. J. Powder Met. and Powder Tech. 20, 1984, pp.115-129.

3. M.L. Wilkins, in "High Energy Rate Fabrication 1984", ed. by I. Berman, J.W. Schroeder, ASME, New York, 1984, pp.63-69.

4. T.C. Peng, S.M.L. Sastry, J.E. O'Neal, and D. Brasher, "Explosive Consolidation of Rapidly Solidified Aluminum Alloy Powders", Metallurgical Transactions A, 16A, 1985, pp.1445-1455.

5. S. Timoshenko, "Strength of Materials. Part II. Advanced Theory and Problems", Van Nostrand, Princeton, New Jersey, 1956.

TABLE I - POWDER REDUCTION SCHEDULE*

Copper	335°C	for 1 hour
	325°C	for 40 minutes
Iron	720°C	for 1 hour
	735°C	for 20 minutes
Brass	285°C	for 40 minutes
	295°C	for 35 minutes
Brass (Samples 19B, 20B, 21B)	425°C	for 35 minutes

* All powders were reduced in hydrogen at the indicated temperatures prior to compaction.

TABLE II. - PARTICLE SIZE DISTRIBUTION (as a percentage)

Size Range (μm)	Copper	Iron	Brass	Sieved Brass
+149	1.811	12.16	5.46	0.00
-149/+104	4.29	17.86	13.45	0.64
-104/+ 74	9.51	21.31	17.37	13.99
- 74/+ 62	12.89	9.17	8.41	6.38
- 62/+ 44	23.41	13.91	12.94	15.03
-44	48.09	25.59	42.37	63.96

TABLE III - POWDER HARDNESS

Material	Hardness (VHN)
Copper	51.5
Iron	80.6
Brass	84.8

TABLE IV - PROPERTIES OF EXPLOSIVES

Explosive	Heat of Explosion (kJ/kg)	Detonation Velocity (km/sec)	Density (g/cm^3)
Detasheet	3400	7.2	1.45
Amatol	4100	5.2	1.6
ANFO	3400	3.2	0.8

TABLE V - AS-COMPACTED COPPER SAMPLES

Sample	Initial Density % Theoretical	Final Density % Theoretical	Energy Absorbing Mandrel	Flyer Plate	Explosives	R*
C1S	41	90	NO	NO	Detasheet	0.6
C2S	41	95	NO	No	ANFO	4.7
CUR	41	95	NO	NO	ANFO	4.7
CURV	46	95	NO	NO	ANFO	4.7
IC	60	93	NO	NO	Amatol	3.3
2C	70	93	NO	NO	Amatol	3.3
3C	47	93	NO	NO	Amatol	3.3
4C	60	95	NO	NO	Amatol	0.8
5C	70	89	NO	NO	Amatol	0.8
6C	70	96	NO	NO	Amatol	1.9
7C	47	95	NO	NO	Amatol	0.8

* R is the ratio of explosive mass to sample tube mass

TABLE VI. - AS-COMPACTED IRON SAMPLES

Sample	Initial Density % Theoretical	Final Density % Theoretical	Energy Absorbing Mandrel	Flyer Plate	Explosives	R*
11	60	98	NO	NO	Amatol	3.3
21	70	99	NO	NO	Amatol	3.3
31	60	99	NO	NO	Amatol	0.8
41	70	96	NO	NO	Amatol	0.8
51	46	99	NO	NO	Amatol	0.8
SR2 1/2	50	98	NO	NO	Amatol	3.3
F2	48	98	NO	NO	Amatol	1.9

* R is the ratio of explosive mass to sample tube mass.

TABLE VII. - AS-COMPACTED BRASS SAMPLES

Sample	Initial Density % Theoretical	Final Density % Theoretical	Energy Absorbing Mandrel	Flyer Plate	Explosives	R*
1B	70	92	NO	NO	Amatol	3.3
2B	60	87	NO	NO	Amatol	3.3
3B	50	95	NO	NO	Amatol	3.3
4B	60	99	NO	NO	Amatol	0.8
5B	70	97	NO	NO	Amatol	0.8
6B	49	98	NO	NO	Amatol	0.8
7B	49	97	NO	NO	Amatol	1.9
8B	50	--	YES	NO	Amatol	0.8
9B THICK	50	97	YES	NO	Amatol	1.9
THIN	50	95	YES	NO	Amatol	
10B THICK	50	97	YES	NO	Amatol	3.3
THIN	50	99	YES	NO	Amatol	
11B THICK	50	98	YES	YES	Amatol	1
THIN	50	97	YES	YES	Amatol	
12B THICK	50	96	YES	YES	Amatol	3
THIN	50	97	YES	YES	Amatol	
13B	50	--	YES	YES	Amatol	8
14B	50	99	NO	YES	Amatol	1
15B	50	99	NO	YES	Amatol	3
16B	50	--	NO	YES	Amatol	8
17B THICK**	60	96	YES	YES	ANFO	4.7
THIN**	60	95	YES	YES	ANFO	
18B THICK**	60	100	YES	NO	ANFO	4.7
THIN**	60	99	YES	NO	ANFO	
19B	60	--	YES	NO	Amatol	1
20B THICK	60	89	YES	YES	Amatol	1
THIN	60	97	YES	YES	Amatol	
21B THICK	60	93	YES	YES	Amatol	3
THIN	60	100	YES	YES	Amatol	

* R is the ratio of explosive mass to sample tube mass.

** These samples were compacted with an altered experimental configuration in which the explosion charge extended above the top of the sample.

TABLE VIII - SHOCK WAVE PRESSURE OF SOME SAMPLES

Sample	End	Explosive* Size (R)	Energy Absorbing Mandrel	Outer Tube	Final Density (%)	Shock Pressure (GPa)
9B	Thick	1.9	Yes	No	96.8	4.6
	Thin				94.5	3.1
10B	Thick	3.3	Yes	No	96.7	4.5
	Thin				98.5	6.4
11B	Thick	1	Yes	Yes	97.5	5.3
	Thin				97.1	4.8
12B	Thick	3	Yes	Yes	95.5	3.7
	Thin				97.1	4.8
14B	-	1	No	Yes	99.3	7.6
15B	-	3	No	Yes	98.9	6.9
6B	-	0.8	No	No	97.9	5.7
7B	-	1.9	No	No	97.4	5.1
3B	-	3.3	No	No	94.7	3.2

*If the sample has an outer tube, R is the ratio of explosive mass to outer tube mass.

If the sample has no outer tube, R is the ratio of explosive mass to sample tube mass.

TABLE IX. - HARDNESS OF AS-COMPACTED SAMPLES (VHN)

Sample	At Core	On Mandrel Side	On Outside
9B			134 (20)*
10B		214 (13)	226 (5)
11B		216 (10)	212 (3)
12B		194 (5)	220 (9)
14B	99.5 (13)		232 (40)
15B	205 (13)		210 (16)
17B THICK			147 (14)
THIN			163 (23)
18B THICK			152 (6)
THIN			170 (5)
20B THICK			85
THIN			172
21B THICK			58
THIN			

*Bracketed values are standard deviations of the measured quantities, usually for 4 or 5 measurements.

TABLE X. - EFFECTS OF SINTERING ON EXPLOSIVELY COMPACTED SAMPLES

Sample	Initial Density (% Theoretical)	Charge Size (R*)	Sintering Temperature** (^{o}C)	L after*** L before	Comments
1B	70	3.3	700	1.01	
			870	0.97	
2B	60	3.3	700	1.00	
			870	0.94	Considerable bulging
3B	50	3.3	700	1.01	some bulging
			870	0.97	some bulging
4B	60	0.8	700	1.00	
			870	1.00	slight bulging
5B	70	0.8	700	1.00	
			870	0.99	
6B	49	0.8	700	1.00	
			870	1.00	
7B	49	1.9	700	1.00	very slight bulging
			870	1.00	

* R is the ratio of explosive mass to container tube mass. The explosive used was Amatol.

** All sintering was for 1/2 hour in hydrogen.

*** L represents the length of the sample before and after sintering.

TABLE XI. - EFFECTS OF SINTERING ON EXPLOSIVELY COMPACTED SAMPLES

Sample	End	Sintering* Temp. (°C)	L after** / L before	Density after Sintering (%)	Hardness**** Before	Hardness**** After
9B	Thick	700	1.00	95	134(20)*****	49(4)
	Thin		0.96	95		61(5)
	Thick	870	0.95	87		68(3)
	Thin		0.96	95		123(34)
10B	Thick	700	1.00	96	226(5)	115(4)
	Thin		0.99	96		106(7)
	Thick	870	***	71		49(3)
	Thin		1.01	64		-
11B	Thick	700	1.00	97	212(3)	126(12)
	Thin		1.00	99		97(5)
	Thick	870	***	43		-
	Thin		***	51		-
12B	Thick	700	1.00	96	220(9)	51(10)
	Thin		1.00	90		104(1)
	Thick	870	1.02	91		71(3)
	Thin		1.02	94		81(12)
14B	-	700	1.00	96	232(40	105(6)
	-	870	***	62		62(6)
15B	-	700	0.99	96	210(16)	104(18)
	-	870	***	62		-

* All sintering was for 1/2 hour in hydrogen.

** L represents the length of the sample before and after sintering.

*** Sample was too irregular to measure.

**** VHN-200 gf Vickers diamond indenter.

***** Bracketed values give the standard deviation of 4 or 5 measurements.

TABLE XII. - GRAIN SIZE DISTRIBUTIONS IN SINTERED SAMPLES

Sample	Sintered (870°C)	Mean Grain Size (μm)	Standard Deviation (μm)
11B	NO	20	24
	YES	30	14
12B	NO	15	14
	YES	14	11
14B	NO	25	19
	YES	32	22
15B	NO	29	17
	YES	30	17
Powder	NO	35.8	28.8

TABLE XIII. - PETRO-FORGE SAMPLES BEFORE SINTERING

Sample	Material	Density (g/cm^3)	% Theoretical
Cu 1	Copper	8.33	92.9
Cu 2	"	8.37	93.4
Cu 3	"	8.38	93.5
Cu 4	"	8.25	92.1
Fe 1	Iron	7.52	95.5
Fe 2	"	7.46	94.8
Fe 3	"	7.49	95.1
Fe 4	"	7.54	95.7
Br 1	Brass	8.17	95.9
Br 2	"	8.23	96.6
Br 3	"	8.18	96.1
Br 4	"	7.98	93.6

TABLE XIV

PETRO-FORGE SAMPLES AFTER SINTERING

Sample	Sintering Temp.(°C)	Diameter Original D	Length Original L	Volume Original V	Density (g/cm)	% Theoretical
Cu 1	744	1.05	1.29	1.20	6.91	77.1
Cu 2	744	1.06	1.20	1.18	7.03	78.5
Cu 3	925	1.01	1.15	1.17	7.10	79.2
Cu 4	925	1.01	1.17	1.12	7.34	81.9
Fe 1	890	0.999	1.007	1.005	7.47	94.9
Fe 2	890	1.001	0.995	0.997	7.49	95.2
Fe 3	1165	1.001	1.000	1.001	7.48	95.0
Fe 4	1165	1.001	1.003	1.004	7.49	95.2
Br 1	700	0.999	1.004	1.002	8.11	95.2
Br 2	700	1.000	1.003	1.003	8.19	96.1
Br 3	870	0.987	1.035	1.009	7.86	92.3
Br 4	870	0.999	1.02	1.018	7.66	89.9

TABLE XV. - HARDNESS OF PETRO-FORGE SAMPLES AFTER SINTERING

Sample	Material	Sintering Temperature (°C)	Hardness*	Original Powder Hardness**
Cu 1	copper	744	30-35	55.5
Cu 3	copper	925	7-10	55.5
Fe 1	iron	890	64-65	72
Fe 3	iron	1165	64-66	72
Br 1	brass	700	61-66	74
Br 3	brass	870	40-59	74

* Rockwell Superficial 15T

** Converted from VHN-25gf to Rockwell Superficial 15T using tables in ASTM E140-83.

TABLE XVI. - FLEXURAL STRENGTH OF PETRO-FORGE SAMPLES AFTER SINTERING

Sample	Material	Sintering Temperature (°C)	Flexural Strength (MPa)
Br 2a	brass	700	84.5
b	brass	700	264
Br 4a	brass	870	240
b	brass	870	260
Fe 2a	iron	890	bottomed out
b	iron	890	601
Fe 4a	iron	1165	bottomed out
b	iron	1165	602

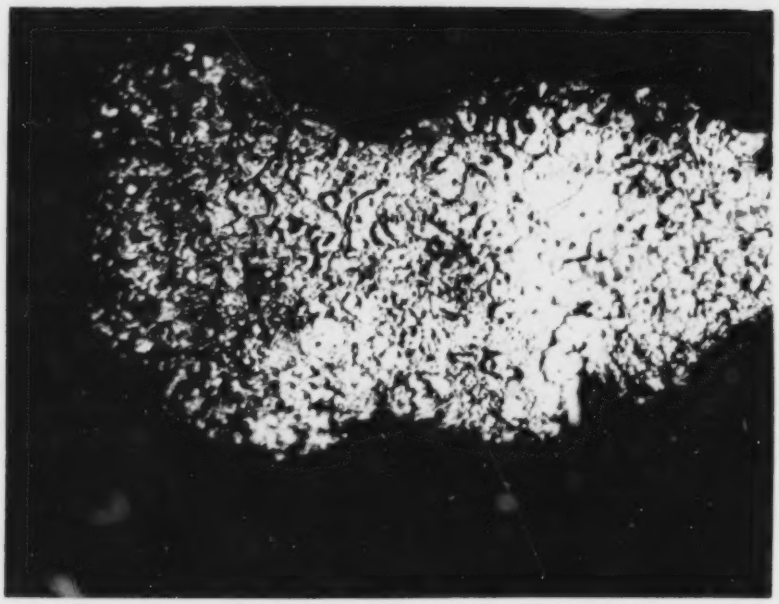

FIGURE 1a

FIGURE 1b

FIGURE 1: Microstructures of the powders to be used in the initial part of this project, magnified 1000 times. The powders are a) copper, b) iron and c) brass

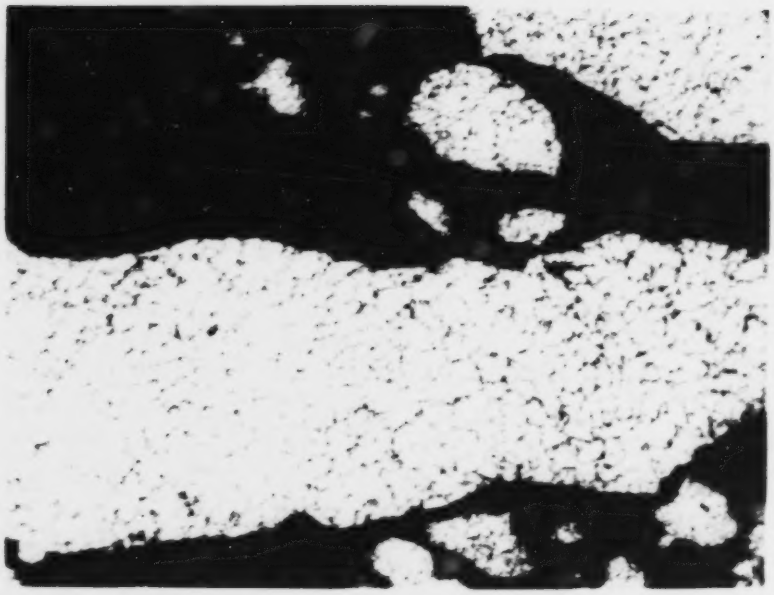

FIGURE 1c

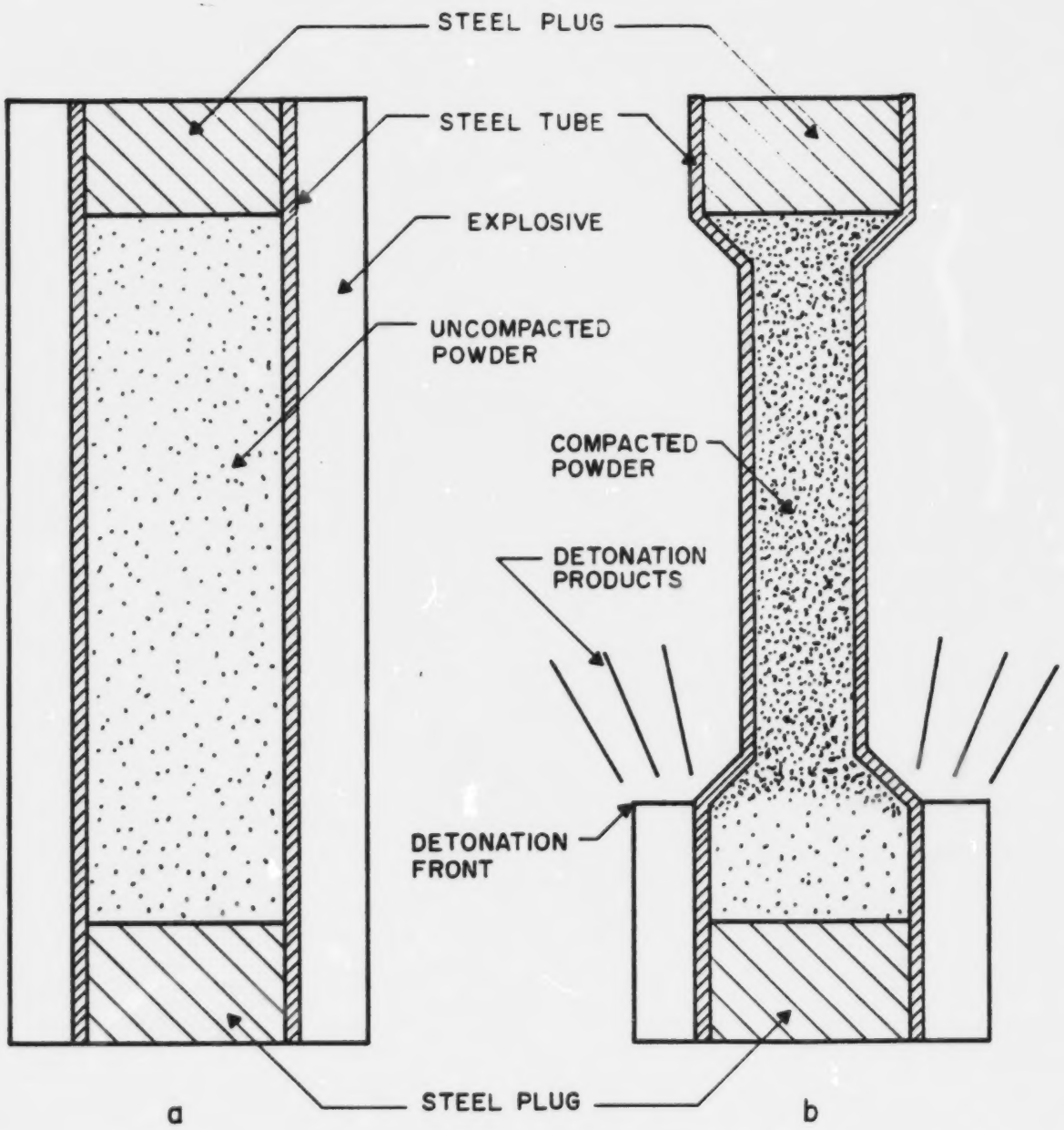

FIGURE 2. Cylindrical compaction geometry a) before detonation, and b) after partial detonation.

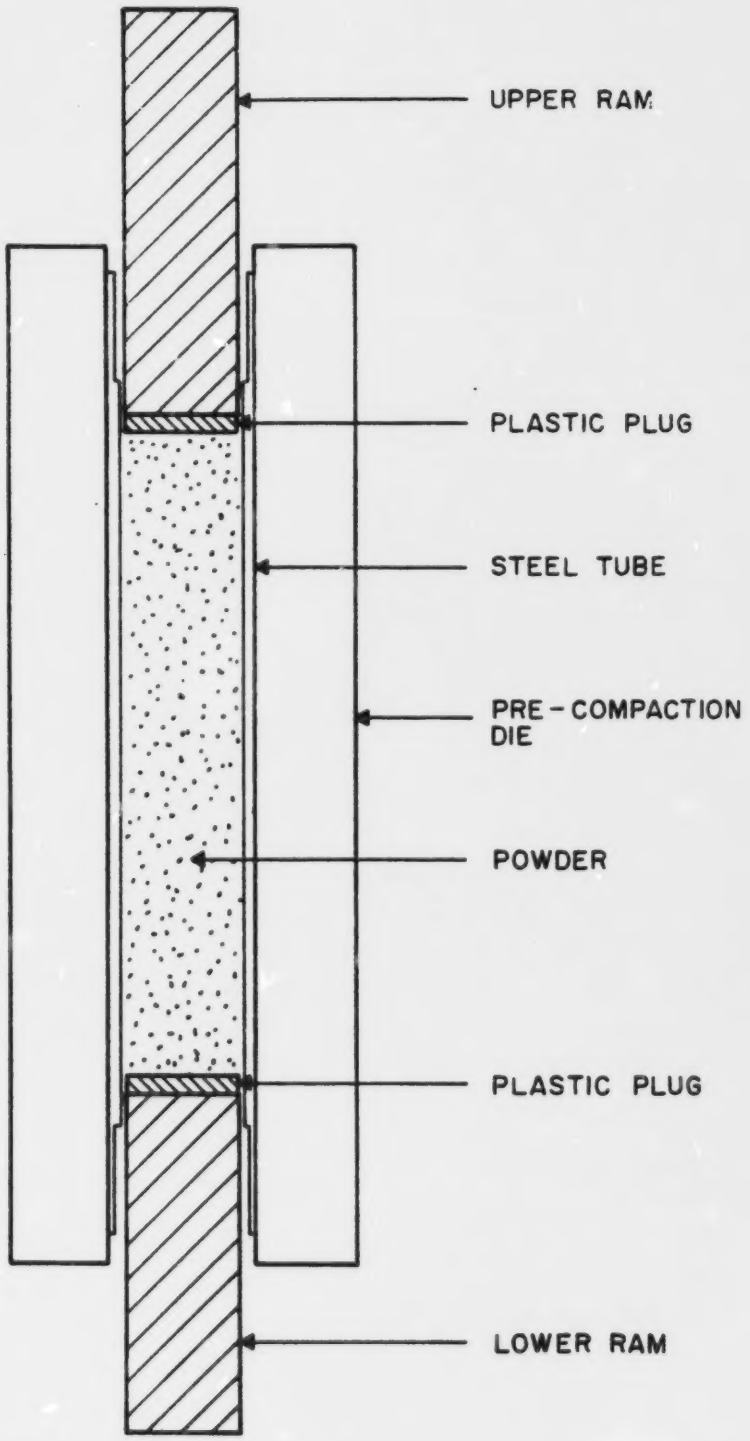

Figure 3. Sample Precompaction Apparatus

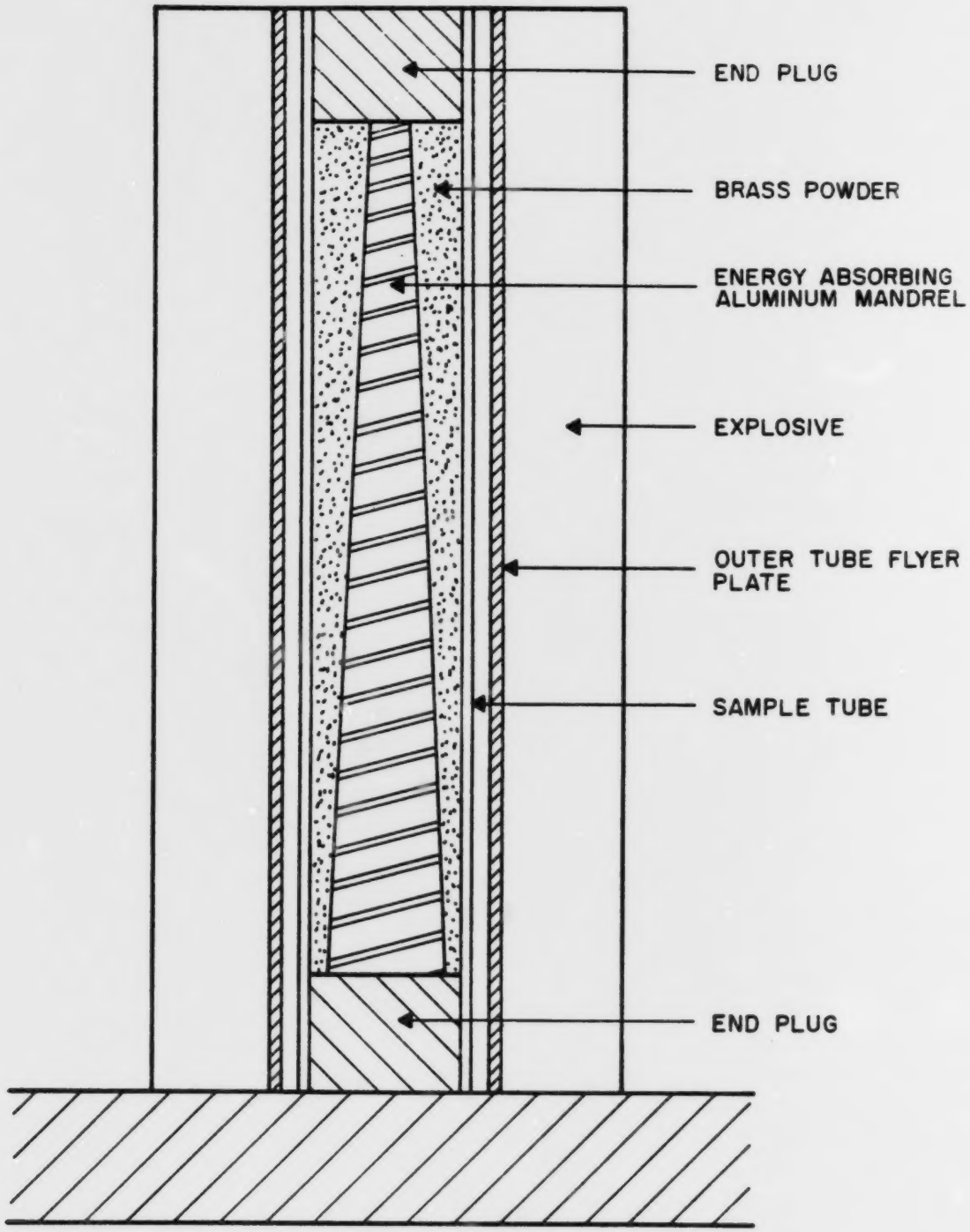

FIGURE 4. Cylindrical sample geometry with central energy absorbing mandrel and outer tube flyer plate.

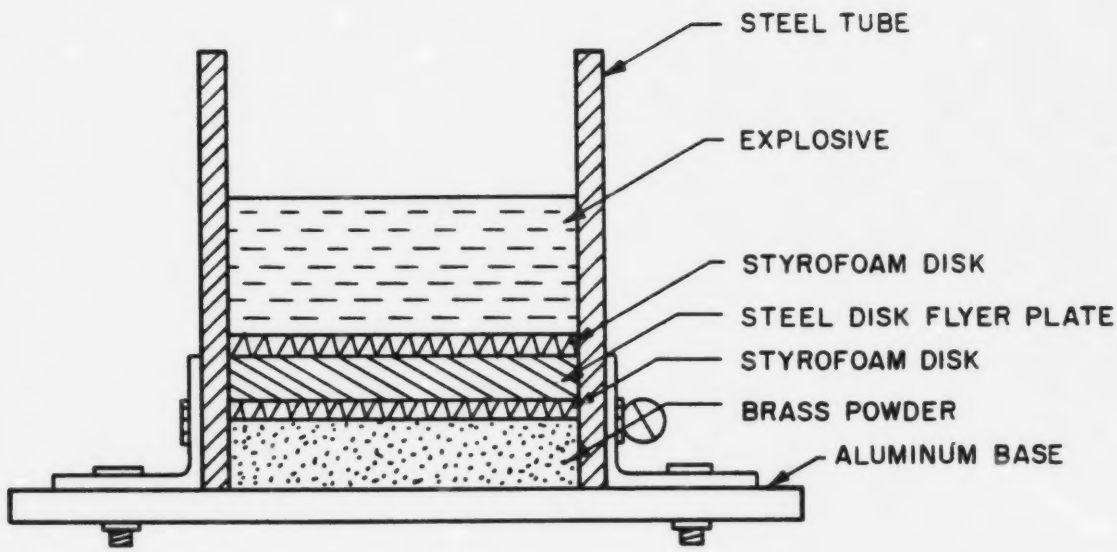

FIGURE 5. Linear compaction sample geometry.

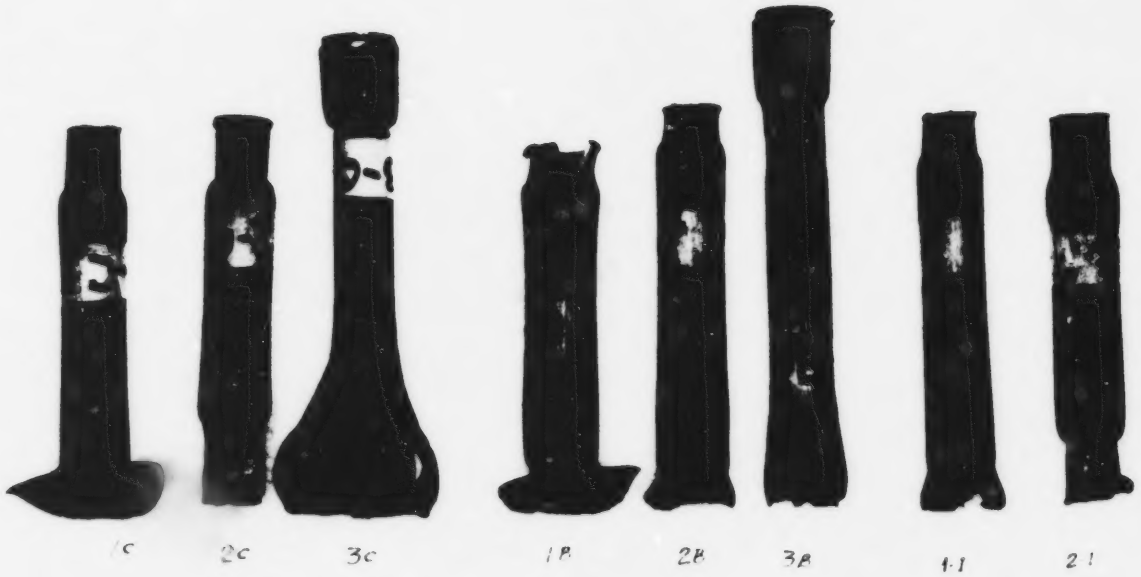

FIGURE 6. Samples after explosive compaction.

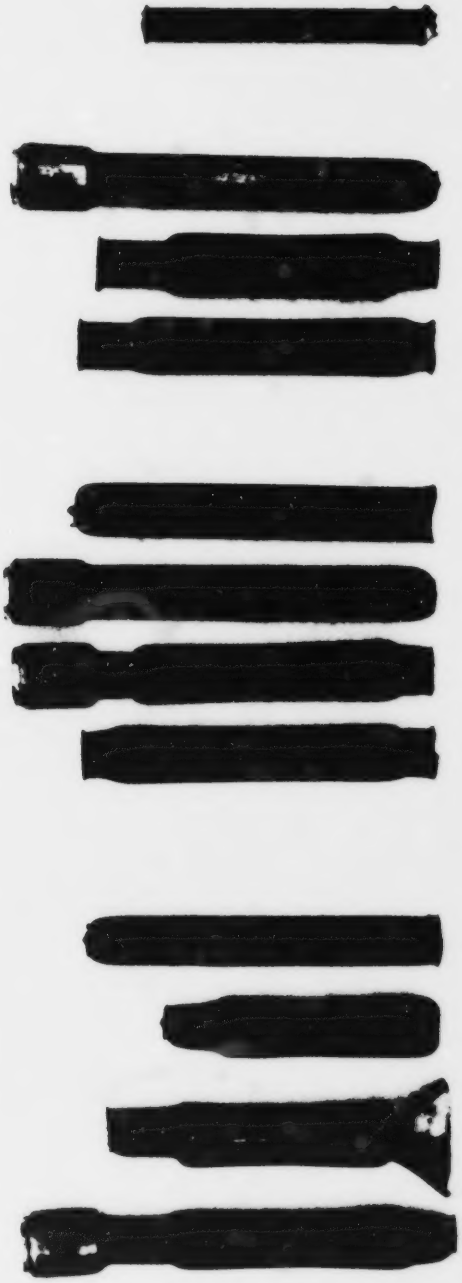

FIGURE 7. Samples after explosive compaction.

FIGURE 8.

Samples after explosive compaction. The apparatus marked "EMPTY" shows (from left to right) the outer tube flyer plate, the sample tube, and the energy absorbing aluminum mandrel. Above and below the mandrel are the steel end plugs which seal the sample tube.

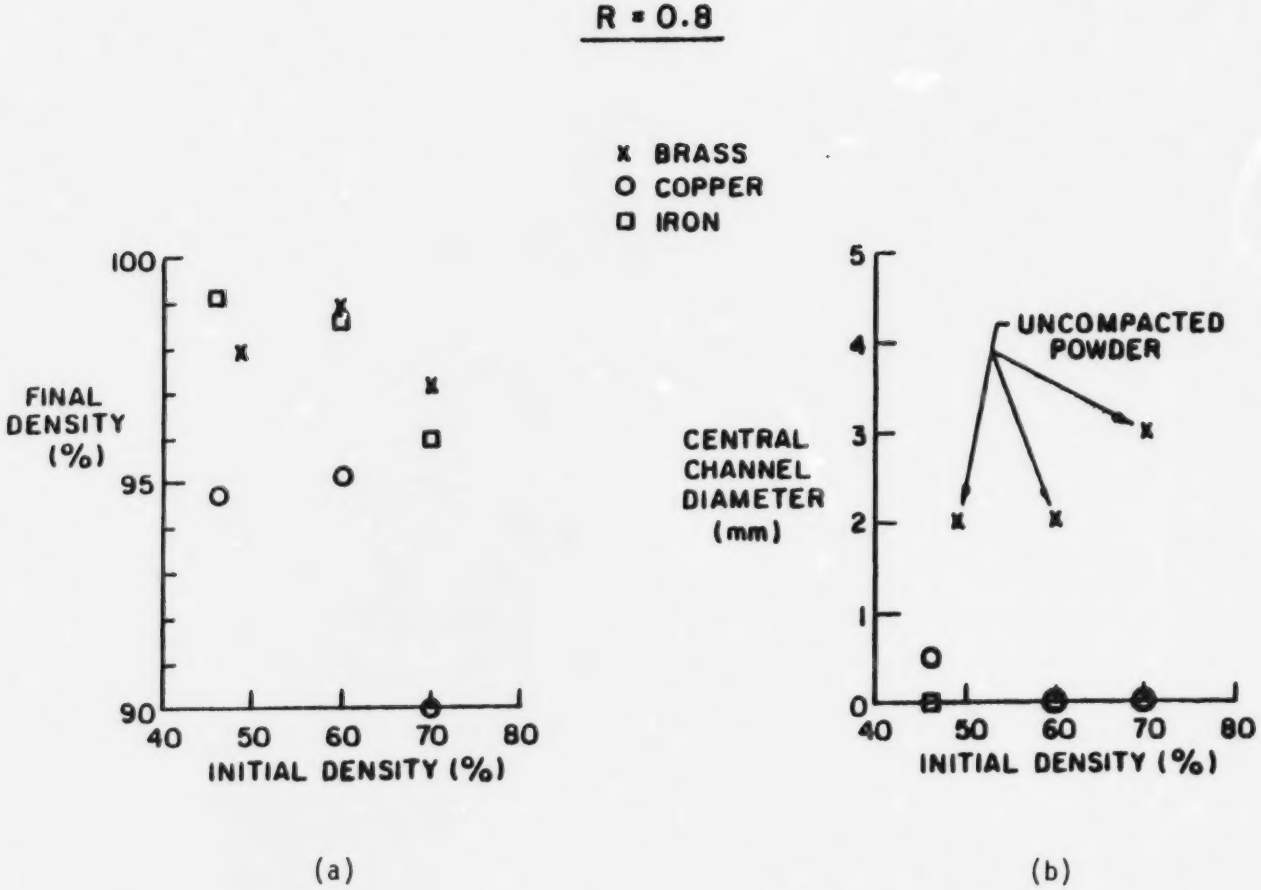

FIGURE 9. The effect of varying the initial powder density with an explosive charge size ratio R = 0.8.

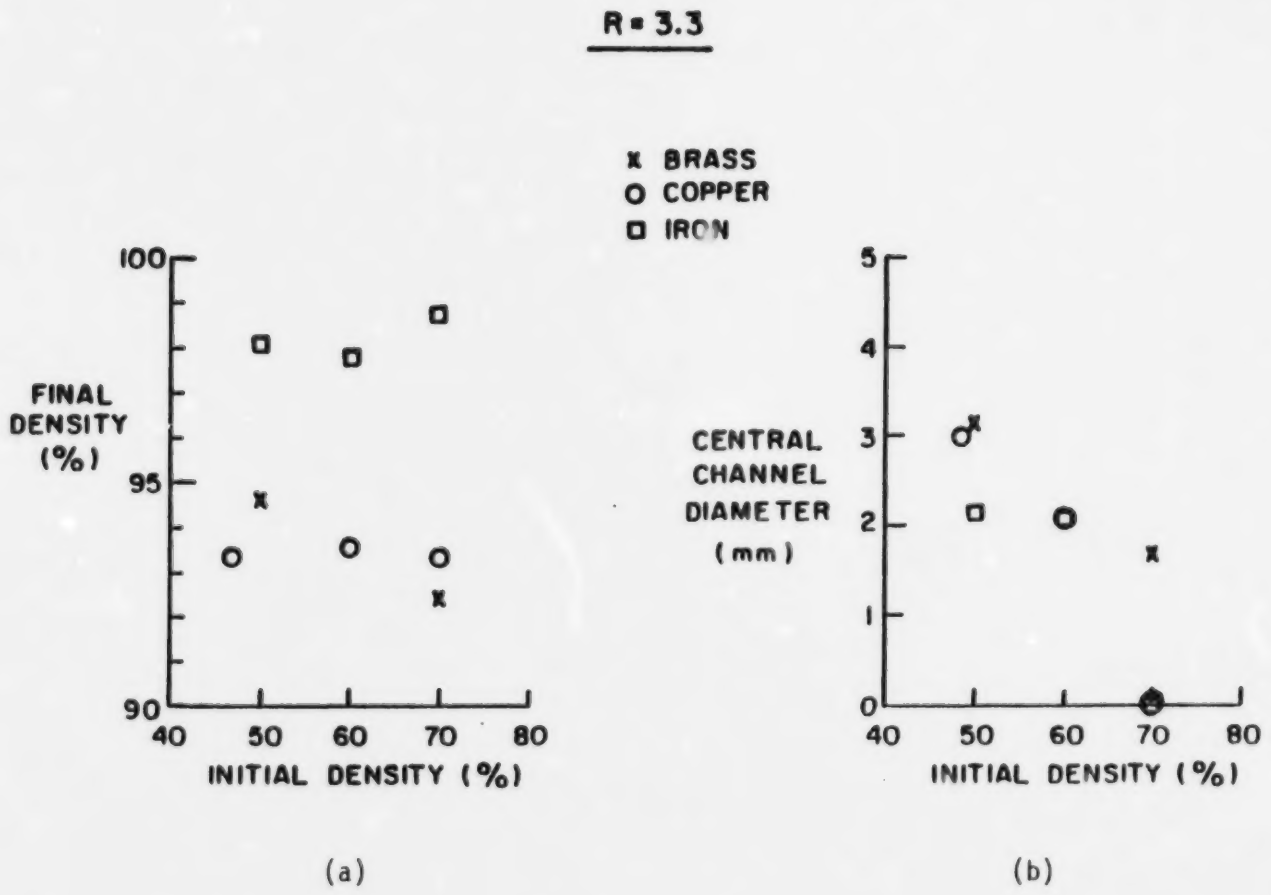

FIGURE 10. The effect of varying the initial powder density with an explosive charge size ratio R = 3.3.

INITIAL DENSITY - 50 %

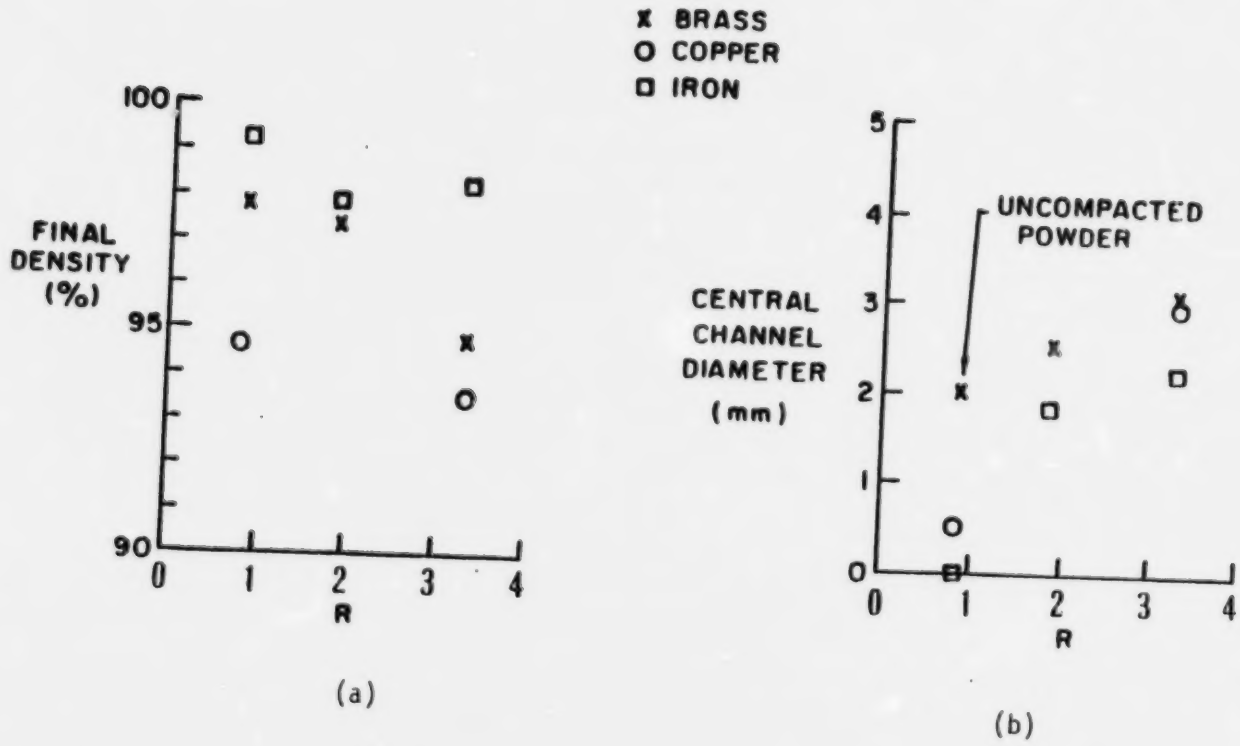

FIGURE 11. The effect of varying charge size ratio (R) with an initial powder density of 50% of theoretical.

INITIAL DENSITY - 70 %

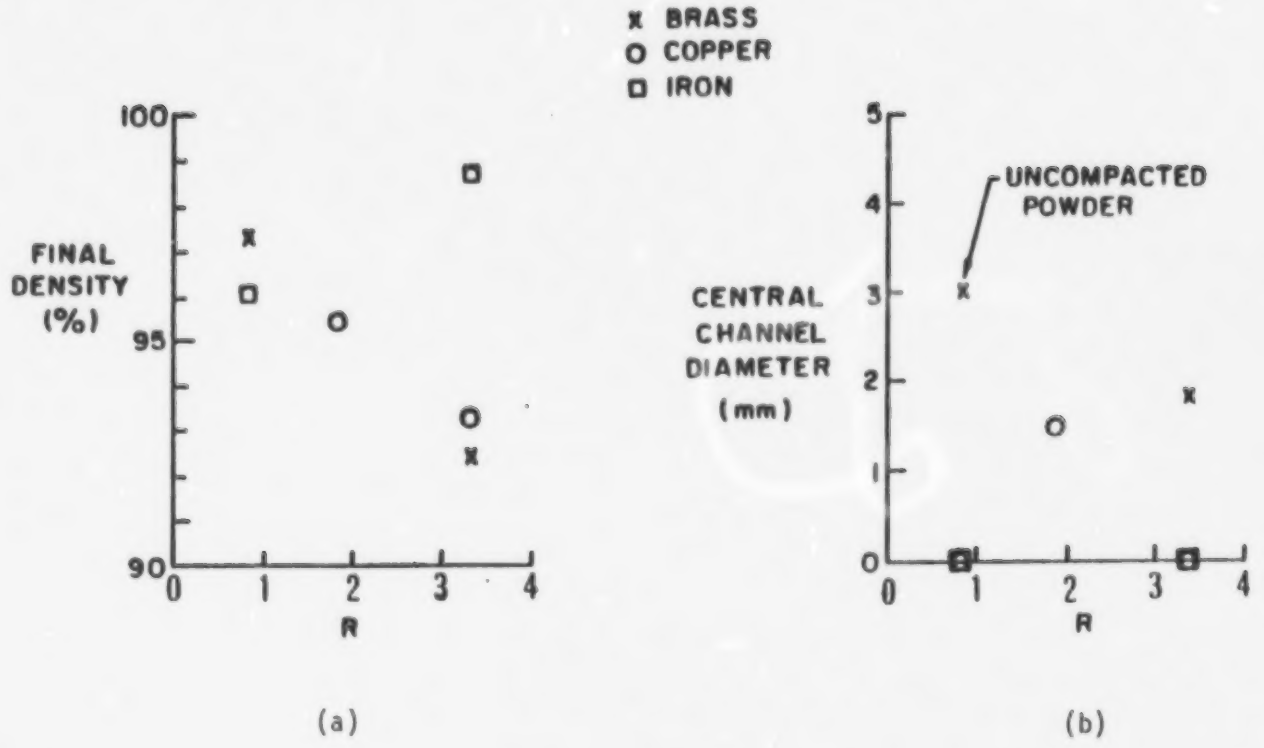

FIGURE 12. The effect of varying charge size ratio (R) with an initial powder density of 70% of theoretical.

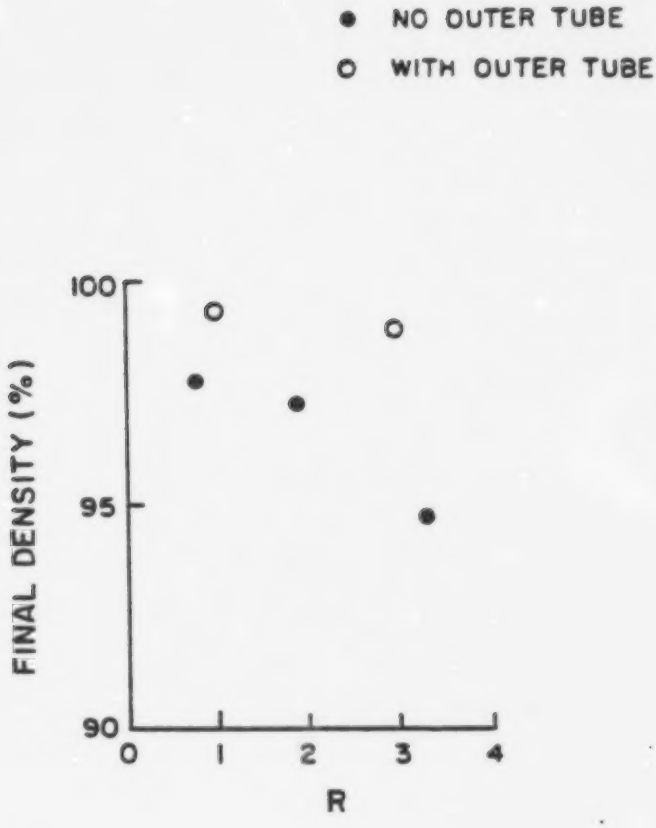

FIGURE 13. The effect a flyer plate has on the final density of the compact. The initial densities of all samples were between 49% and 50%.

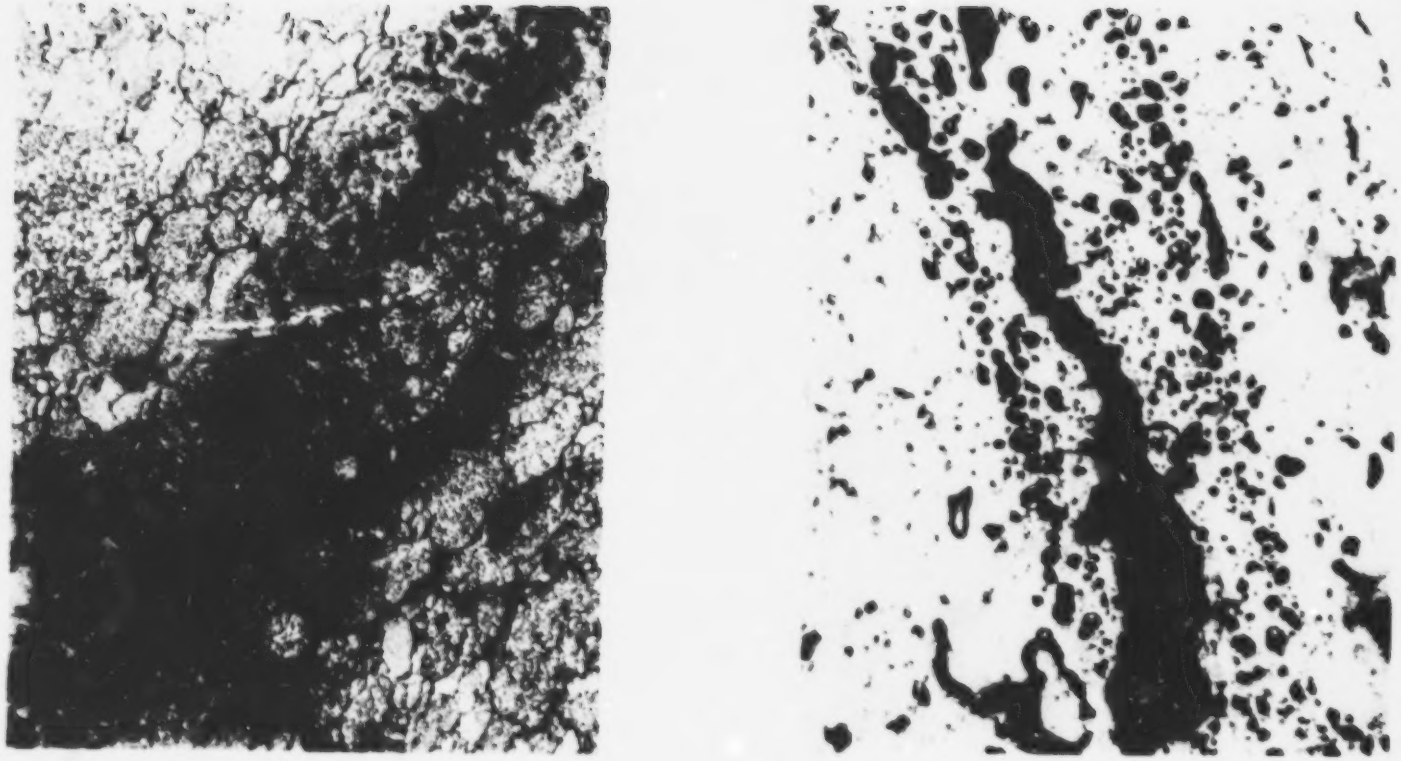

(a) (b)

FIGURE 14. Sample 12B, inside edge, X250: a) unsintered, b) sintered at 870°C.

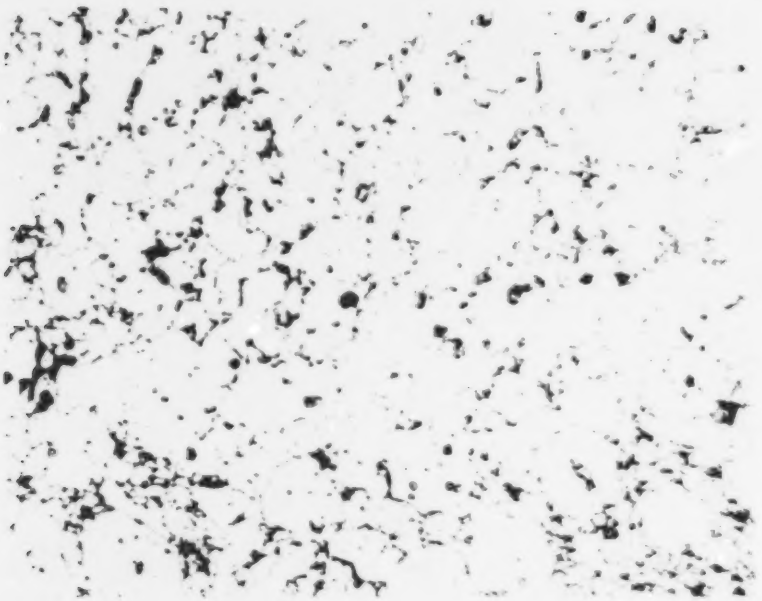

(b)

(a)

FIGURE 15. Sample 12B, outside edge, X250: a) before sintering, b) sintered at 870°C.

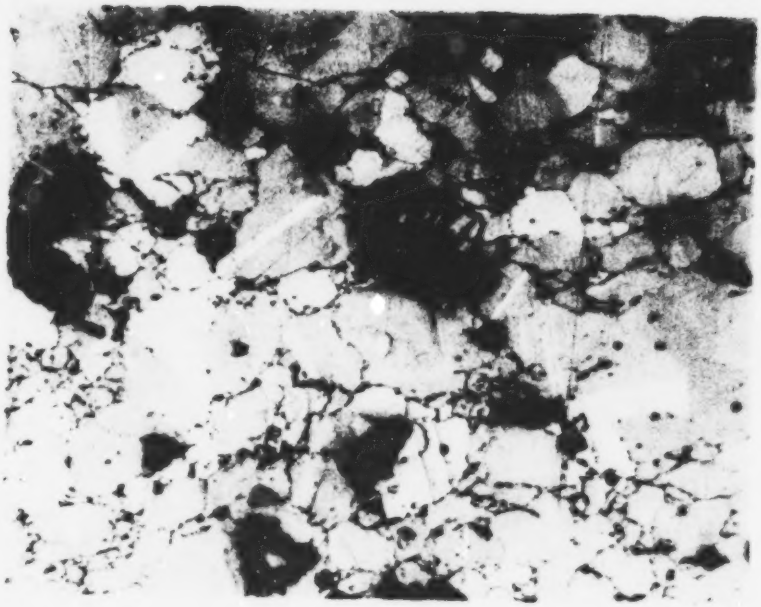

(b)

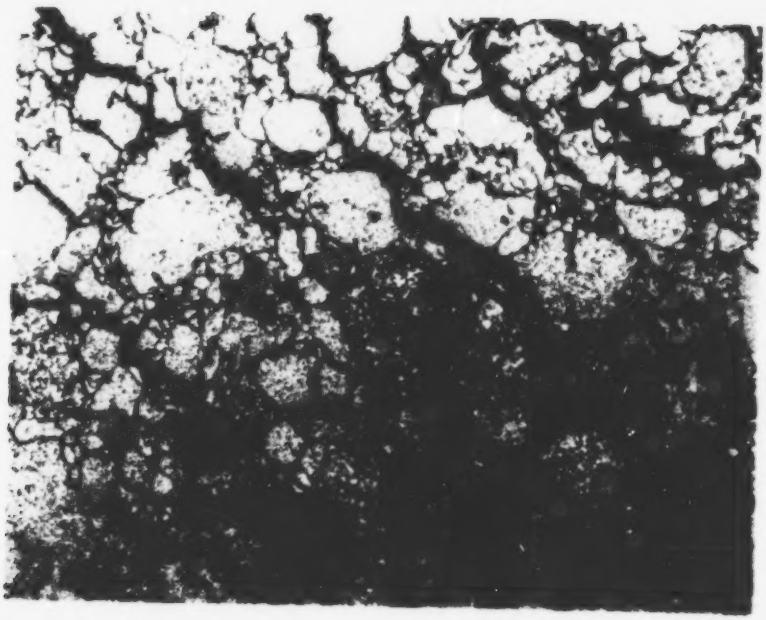

(a)

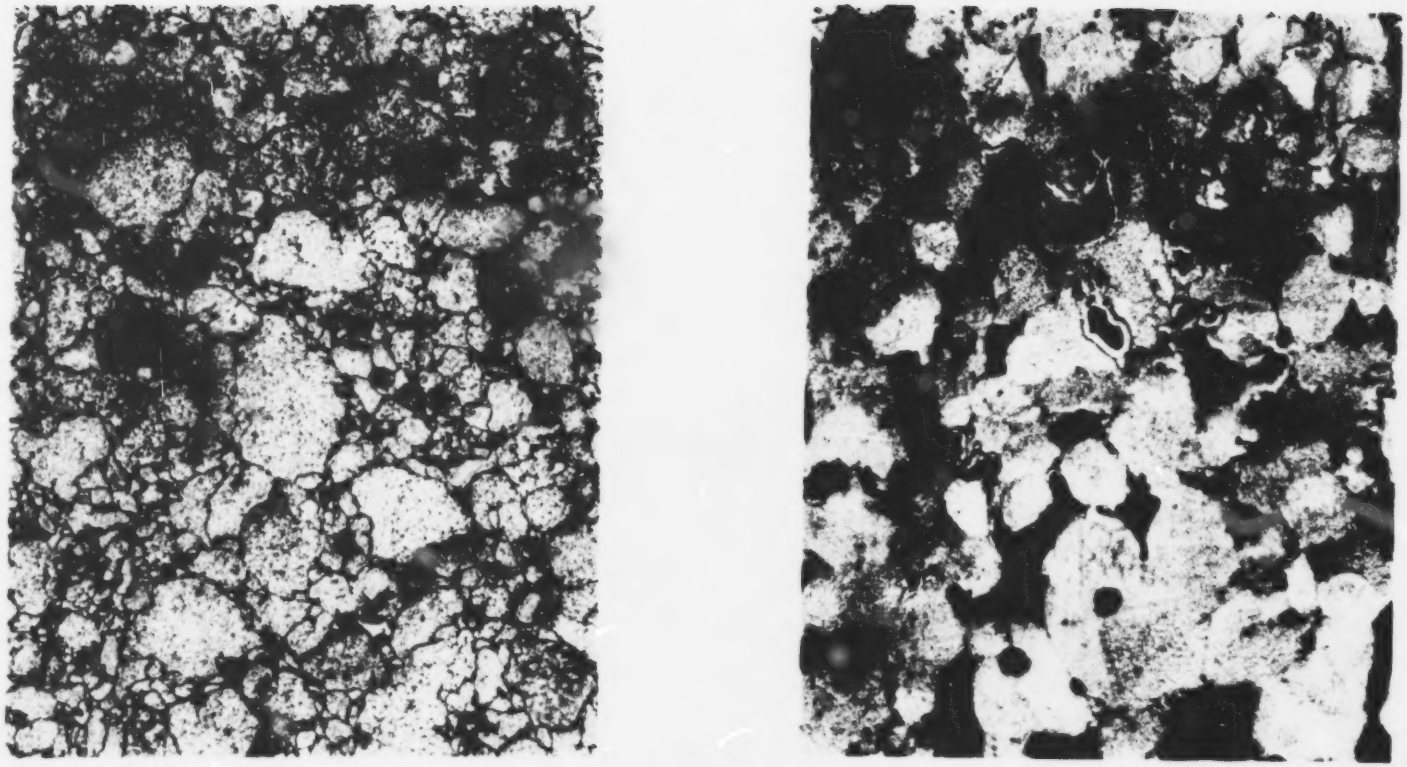

(a) (b)

FIGURE 17. Sample 15B, outside edge, X250: a) unsintered, b) sintered at 870°C.

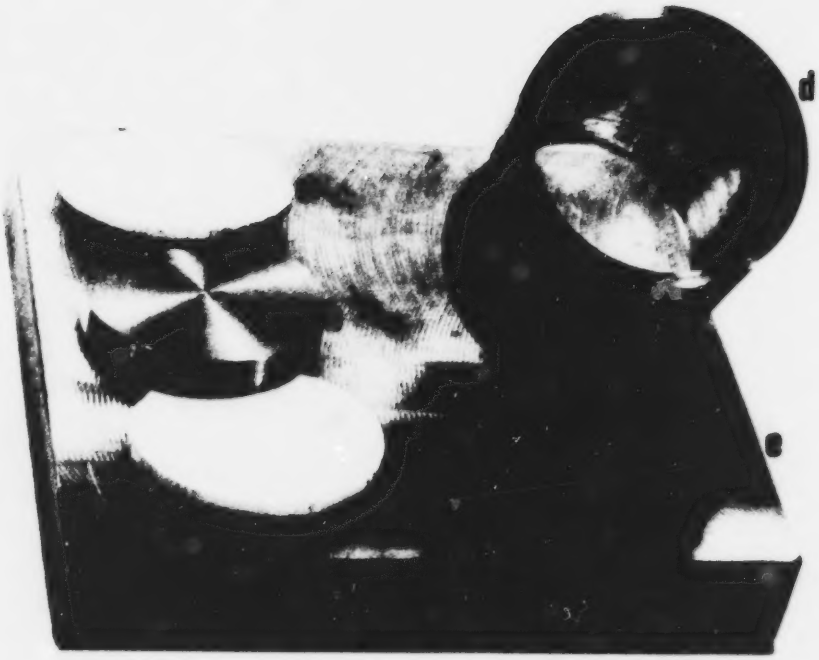

FIGURE 18. Linear explosive compaction apparatus. The components are: a) styrofoam disk, b) metal disk flyer plate, c) styrofoam disk, d) cylindrical tube and e) a metal base.

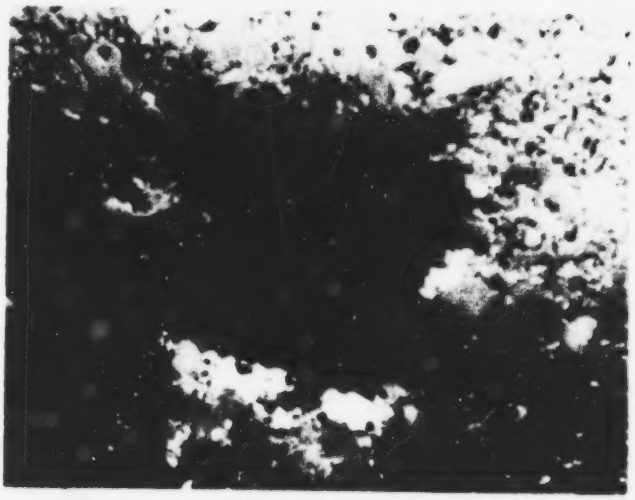

(a)

(b)

FIGURE 19. Vickers hardness impression (20 kg load) in brass samples. a) Linear compaction sample, b) cylindrical sample 12B, c) cylindrical sample 15B, d) wrought brass (x74).

19 (c)

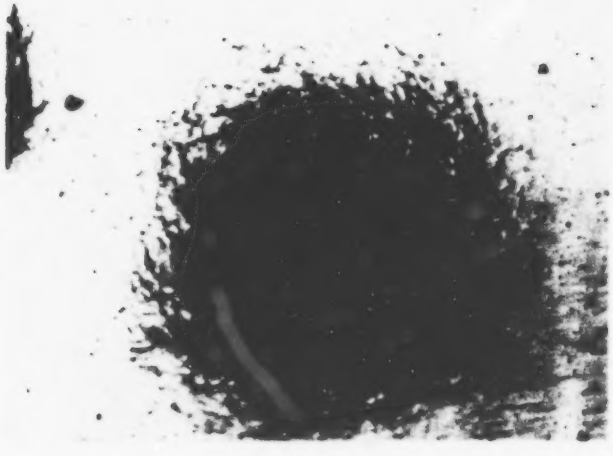

19 (d)

APPENDIX I.

"SHOCK WAVES"

SHOCK WAVE

A shock wave passing through a sample causes what might be described as an instantaneous change in state. The actual width of the shock front in a powder sample is approximately the size of a powder grain [1]. Consider a shock wave passing at a speed v_s through a stationary sample of initial density d_o, initial pressure P_o and initial energy E_o. The final particle speed is v_p (the speed of the bulk motion of the compact), the final density is d, the final pressure is P and the final energy is E (See Figure 1). The equations relating these quantities before and after the shock wave are called the Rankine-Hugoniot equations[2]. The equation governing conservation of mass is

$$d_o \; v_s = d \; (v_s - v_p) \tag{1}$$

that governing transfer of momentum is

$$P - P_o = d_o \; v_s \; v_p \tag{2}$$

and that governing transfer of energy is

$$E - E_o = \frac{P_o}{d_o} \; \frac{v_p}{v_s} + \frac{v_p^2}{2} \tag{3}$$

Eliminating v_s and v_p from the above equations results in the Hugoniot energy equation

$$E_o - E = \frac{(P + P_o)}{2} \left(\frac{1}{d_o} - \frac{1}{d} \right) \tag{4}$$

which is often written

$$E_o - E = \frac{(P + P_o)(V_o - V)}{2} \tag{5}$$

Appendix 1.

where V, the reciprocal of d, is the specific volume, the usual experimental procedure is to measure v_s, d_o and d. With this information, v_p is calculated from (1), P is then calculated from (2), and finally E from either (3) or (4).

For a specific shock wave velocity and pressure, the final state is determined unambiguously from the initial state. Thus, equations (1) through (5) represent equations of state. The equations of state (or Hugoniots) for a number of solid materials have been measured[2], as well as those for a number of porous samples[2,3,4,5]. Hugoniots are shown schematically in Figure 2. Figure 2a shows a Hugoniot for a solid and Figure 2b that for a powder (or porous) sample.

The change in state which occurs on the passage of the shock wave is irreversible since it results in the dissipation of energy. The amount of energy dissipated in the process is approximately given by the shaded regions in the curves in Figure 2[6]. The curves marked H represent Hugoniots for the particular sample being shocked and the curves marked R represent straight lines between the state conditions immediately before and immediately after the shock wave front. These straight lines are also known as Rayleigh lines. The curve marked S in Figure 2b is the solid Hugoniot.

Above a certain compaction pressure (P_c), the powder sample will be compacted to the solid density, and the Hugoniot can be approximated by the solid Hugoniot. P_c is dependent on the material being compacted, but is not (strongly) dependent on the initial sample density. For example, copper powder is fully compacted by a shock pressure of about 21 kbar[3] and tungsten by about 45 kbar[5].

SHOCK WAVE SOURCES

Shock waves are usually generated by impacting a sample with a highspeed projectile or with an explosion. Each of these methods has advantages and disadvantages.

Appendix 1.

The use of projectiles has the advantage that the energy and the momentum of the collision can be adjusted independently. This is done by changing the projectile mass and velocity. Having these degrees of freedom is very useful in controlling the compaction process. The disadvantage of using projectiles is that a gun or accelerator is necessary to impart the energy into the projectile. At the high speeds used in shock wave compaction, the guns tend to be very large and expensive.[7].

Explosives are a less expensive source of shock waves than are projectiles. Explosive shock waves are, however, less well controlled than those from projectile impacts. The variables are explosive burn velocity and explosive mass (or energy). The burn velocity is determined by the explosive type and thus can not be set at any arbitrary value. Because of the lower expense involved in explosive compaction, this is the preferred method to be used in initial compaction trials.

Appendix 1.

REFERENCES

1. W.H. Gourdin, J. Appl. Phys. 55, 1984. pp.172-180.

2. R.G. McQueen, S.P. Marsh, J.W. Taylor, J.N. Frite and W.J. Carter, in "High-Velocity Impact Phenomena", ed. by R. Kinslow, Academic Press, New York, 1970. pp.293-417.

3. R.R. Boade, J. Appl. Phys. 39, 1968. pp.5693-5702.

4. R.R. Boade, J. Appl. Phys. 40, 1969. pp.3781-3785.

5. R.R. Boade, J. Appl. Phys. 41, 1970. pp.4542-4551.

6. "Dynamic Compaction of Metal and Ceramic Powders", Report of the Committee on Dynamic Compaction of Metal and Ceramic Powders, National Academic Press, Washington, D.C., 1983.

7. A.J. Cable, in "High-Velocity Impact Phenomena", ed. by R. Kinslow, Academic Press, New York, 1970. pp.1-21.

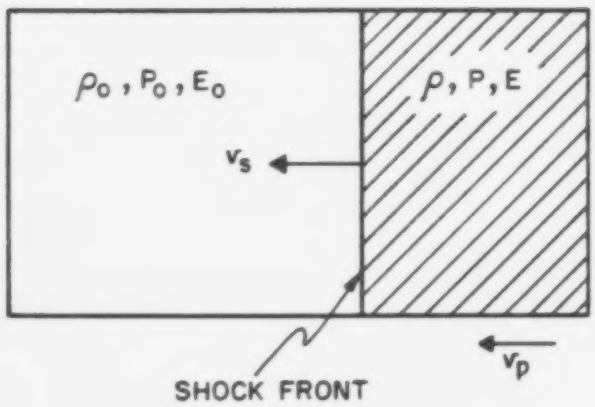

FIGURE 1. A shock wave passing through an object which is initially at rest.

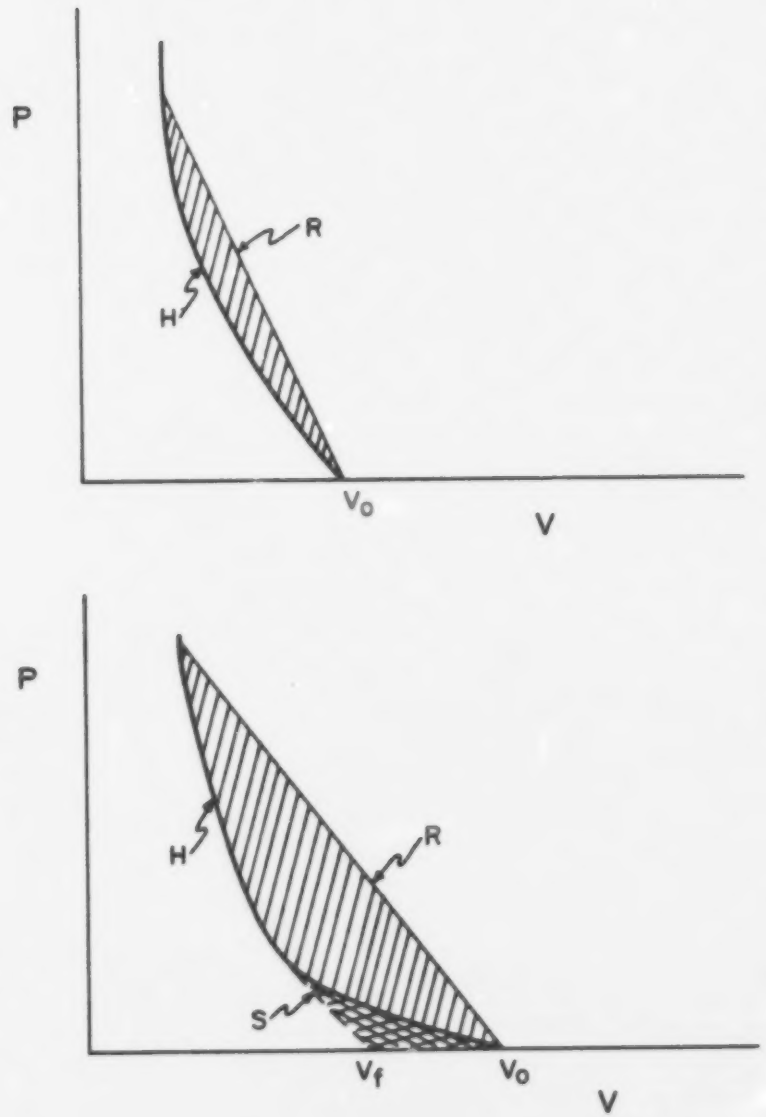

FIGURE 2. Hugoniots relating pressure and specific volume. Figure 2a shows the curve for a solid sample and Figure 2b shows the curve for a powder sample made up of the same material as in 2a. Curves marked H are Hugoniots, curves marked R are Rayleigh lines, and the curve marked s represents the solid Hugoniot.

APPENDIX II.

"SHOCK WAVE COMPACTION GEOMETRIES"

Appendix 2.

SHOCK WAVE COMPACTION GEOMETRIES

Compaction by shock waves makes use of basically two geometries, described here as linear compaction and cylindrical compaction (these notations have been coined for this report). Each of these geometries is described below.

Linear Compaction

A schematic diagram of linear compaction is shown in Figure 1. In this type of compaction, the shock wave enters the powder from one side, passes through the sample and leaves through the opposite side. The sample need not be rectangular in shape; simple dies can be used to produce shaped components[1].

Notice that after the passage of the shock wave, the compacted sample has a velocity v_p. The example shown in Figure 1 is a scale representation of a typical compaction process in which the initial powder density is one half of the final density. For this case, the final velocity of the compacted sample is one half of the shock wave velocity. Typical shock wave velocities are about 1500 m/sec, so typical compact velocities would be about 750 m/sec. This is more than twice the speed of sound in air (the final compacted sample is travelling at more than Mach 2). As a result, momentum traps are necessary to slow the sample down in a manner which does not damage it. This type of compaction can be used with shock waves generated by either projectile impact or by explosion.

Cylindrical Compaction

A schematic diagram of a cylindrical compaction is shown in Figure 2. This diagram shows a cross sectional view of a cylinder being compacted. Because of the geometry of the sample, projectiles can not be easily used, and explosives are the practical method of generating the shock wave. The

Appendix 2.

explosives are packed around the cylindrical sample and ignited from one end to the other. Thus the explosive shock hits equally and at the same time around the circumference of the cylinder and travels along the length of the cylinder.

In this compaction geometry, the compacted material is still moving with a velocity v_p, but now this material is moving towards the centre of the cylinder. There is a build-up of energy in the centre as the material from opposite sides of the cylinder collides. This results in a structurally damaged region along the middle of the cylinder. This region is called the Mach Stem [2, 3]. Notice that the Mach Stem is not produced by using too much energy in the compaction process, it is the result of using shock waves to compact a powder sample. Thus, the cylindrical geometry is not desirable if the entire volume of the compacted part must be uniform. One method of minimizing the extent of the Mach Stem may be to put an energy absorbing material along the centre of the original powder. This would result, however, in a compact which is not uniform throughout, but which has a core made up of another material.

Appendix 2.

REFERENCES

1. D. Raybould, Powder Metallurgy, 25, 1982. pp.35-41.

2. M.A. Meyers and B.B. Gupta, Journal of Metals, October, 1981. pp.21-26.

3. "Dynamic Compaction of Metal and Ceramic Powders", Report of the Committee on Dynamic Compaction of Metal and Ceramic Powders, National Academic Press, Washington, D.C., 1983.

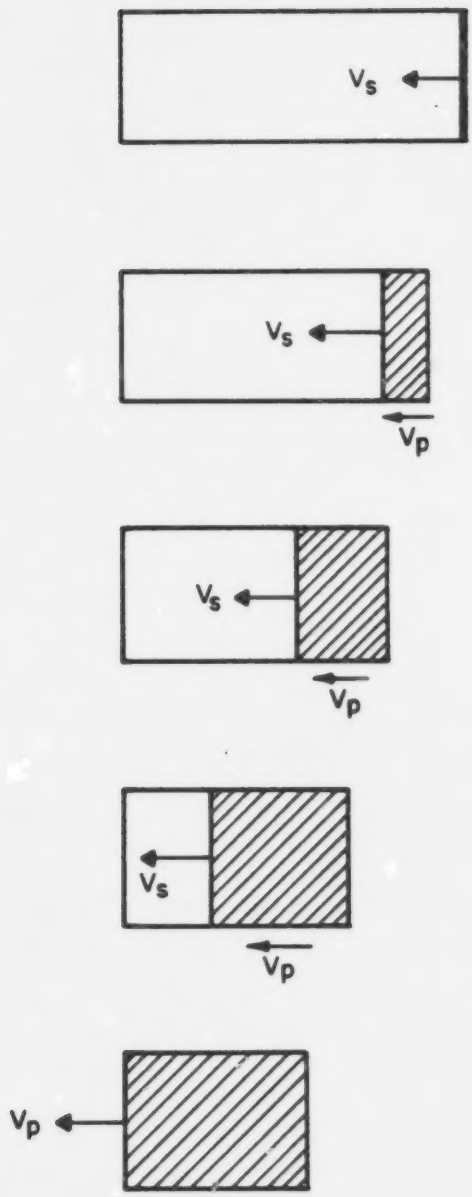

FIGURE 1. Linear compaction. This is a scale drawing for the case in which the final density is twice the initial density. Shaded areas are behind the shock front.

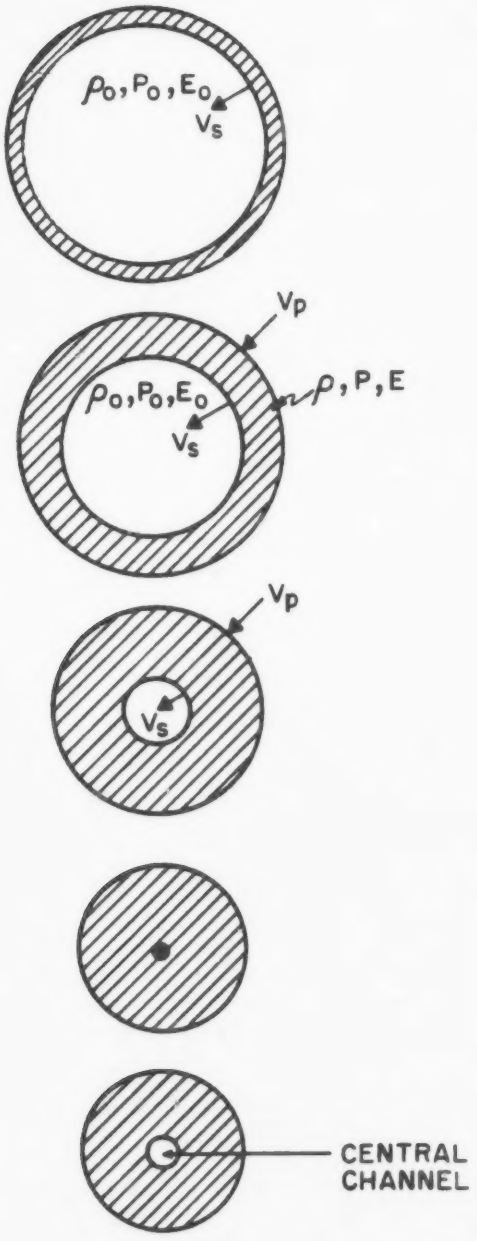

FIGURE 2. Cylindrical compaction. Shaded areas are behind the shock front.

APPENDIX III.

"PARTICLE SURFACE TEMPERATURE AND COMPACTION RATE"

PARTICLE SURFACE TEMPERATURE AND COMPACTION RATE

The energy which is used to compact a powder goes into two basic processes. One process involves compressing the powder (and thus increases the bulk kinetic energy of the sample) and the other involves raising the temperature of the compacted specimen. If the velocity of the compaction wave is large, then most of the heating occurs at the surfaces of the particles. The particle surface temperature is given by[1]

$$T_s = T_o + \frac{E}{C_p} + \frac{v_s E \rho_o}{6K} d \left[0.1 - \sum_{\eta=1}^{\infty} \frac{1}{X_\eta^2} \exp\left(\frac{-4 \alpha X_\eta^2}{v_s d} \right) \right]$$

where T_s is the maximum surface temperature
T_o is the initial powder temperature
v_s is the speed of the compaction shock wave
E is the deposited energy per unit mass

$d = \frac{\Delta^2}{D}$ where $\Delta = \frac{6}{\rho_o A}$ A the measured surface area per unit mass of powder and D is the particle diameter.

ρ_o is the solid density
K is the thermal conductivity of the material
X_η is the nth root of the equation $\tan X_\eta = X_\eta$
α is the thermal diffusivity of the material

For most practical cases of interest, only the first term in the sum in equation 1 need be considered and, for this term, X≈4.5. In this limit, the factor in the square bracket in equation 1 will range from 0.10 (for v_s small) to 0.05 (for v_s large). This equation is shown plotted in Figure 1 for a copper powder with a (uniform) diameter of

40μm. For a uniform system d = D. The energy deposited in the sample is 77 KJ/Kg, enough to raise the bulk temperature of the sample by 200°C. The initial powder temperature is assumed to be 0°C. In order to achieve surface temperatures of the order of the melting temperature of copper (1083°C), it is necessary to go to shock wave velocities of the order of 3000 m/sec. This velocity is in the range of explosive compaction.

REFERENCE

1. W.H. Gourdin,J. Appl. Phys. 55, p.172, 1984.

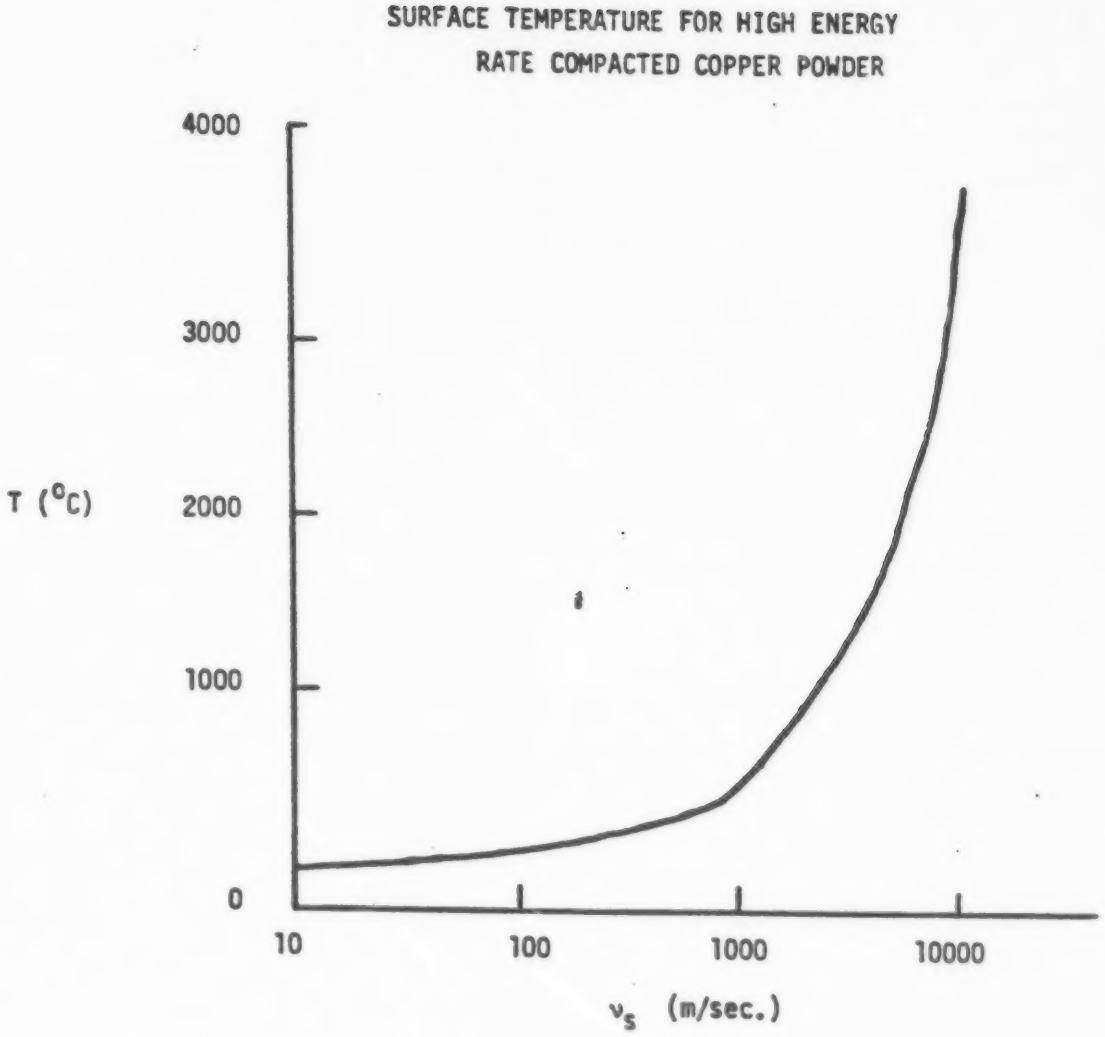

FIGURE 1. Surface temperature of copper particles as a function of shock wave velocity. The particles have a (uniform) diameter of 40μm and a total energy of 77 KJ/kg is deposited during compaction.

APPENDIX IV.

"SHOCK WAVE PRESSURES"

Appendix: Shock Wave Pressures

List of Symbols:

S, Co	Shock-wave parameters
v_s	Shock-wave velocity
v_p	Particle velocity
ρ_o	Initial powder density
ρ	Final density
P	Shock pressure
Po	Ambient pressure before shock-wave

Assume a linear relationship between v_s and v_p, of the form

$$v_s = Co + Sv_p \qquad (1)$$

From tables on page 517 of reference 1, the following values of Co and S can be calculated:

Copper at 51% of theoretical density

Co = 0.171 km/sec
S = 1.836

Iron at 43% of theoretical density

Co = 0.139
S = 1.725

In these calculations, it will be assumed that the values for brass are

Co = 0.17 km/sec
S = 1.8

A comparison with measured data in reference 2 shows that these are reasonable values.

From conservation of mass,

$$\rho_o \, v_s = \rho(v_s - v_p) \tag{2}$$

Equations (1) and (2) can be combined to give the result

$$v_p = \frac{\rho_o - \rho}{(\rho - \rho_o)S - \rho} \quad Co \tag{3}$$

The equation describing transfer of momentum is

$$P = Po + \rho_o \, v_s \, v_p \tag{4}$$

Relative to shock pressures, Po = 0. Solve equation (2) for v_s, substitute into equation (4), and set Po = 0 to obtain

$$P = \frac{\rho_o \, \rho}{\rho - \rho_o} \, v_p^2 \tag{5}$$

In this equation, v_p can be obtained from equation (3), giving P as a function of ρ for fixed ρ_o. A plot of equation (5) for an initial density of 49% of theoretical is shown in Figure A1.

References

1. "High-Velocity Impact Phenomena", ed by R. Kinslow, Academic Press, New York, 1970.

2. R.R. Boade, "Compression of Porous Copper by Shock Waves", J. App. Phys. 39, 1968. pp 5693-5702.

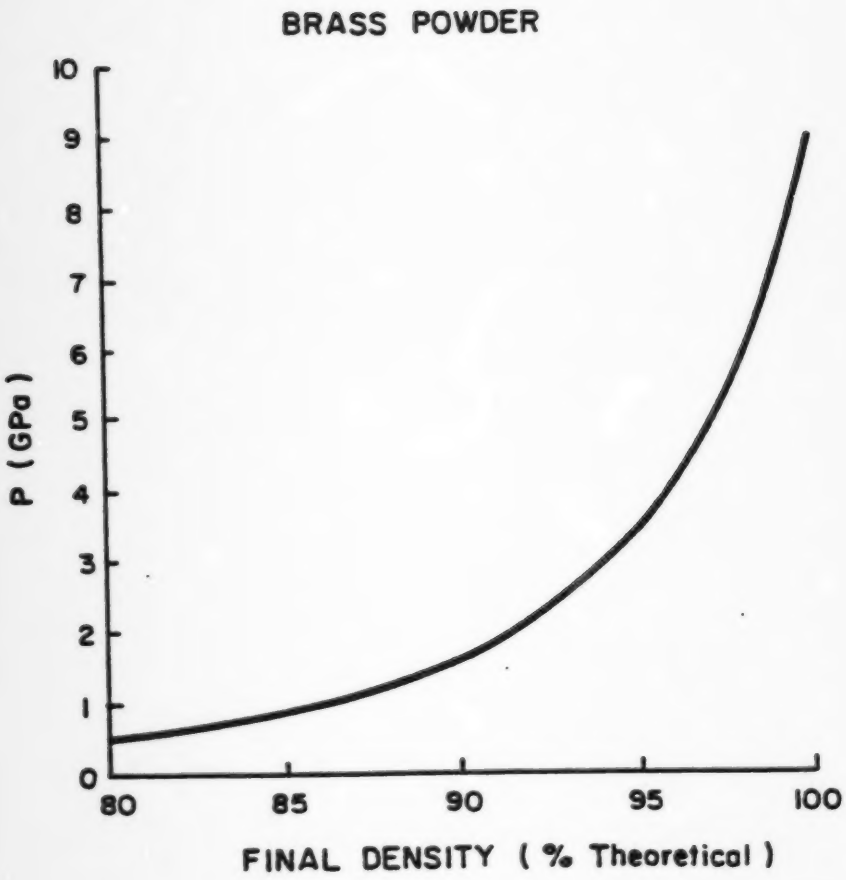

FIGURE A1. Shock wave pressure as determined from the final sample density for brass. Initial density is 49%.

APPENDIX V.

"CALCULATING EFFECTIVE EXPLOSIVE CHARGE SIZES"

Final Report
Limpact Industries Limited

Calculating Effective Explosive Charge Sizes

The process of imparting energy into a work piece, through the detonation of an explosive, is a complicated process. An understanding of this process is hampered by the high speed at which it takes place, and by the hazardous nature of an explosive event. A number of engineering formulae are used to calculate the amount of energy transferred from an explosive to a work piece, and these formulae are discussed in this appendix. This topic is discussed in detail in the references [1,2].

The traditional geometry considered is that of an explosive welding process, in which one of the sections to be welded is accelerated into the other. The accelerated component is called the flyer plate and the stationary component is called the parent plate. The energy transferred to the system is the kinetic energy of the flyer plate. The quantity calculated is the velocity of the flyer plate, Vp.

The effective energy density of the explosive is designated E, and the flyer plate velocity is given by

$$Vp = \sqrt{2E}\ f(R)$$

where R is the ratio of explosive mass to flyer mass, and f(R) is a function which depends on the geometry of the set-up. Examples of forms for f(R) can be found in equations 4.12 and 4.13 of [1].

The value of E is not simply related to the caloric energy density of the explosive. For low density explosives, the value of E is a smaller fraction of the caloric energy density than for high density explosive. Table I lists the properties of some explosives.

Rather than using equations to calculate Vp, a nomograph can be used. An example of such a nomograph for a flat geometry (taken from [2] is shown in Figure 1. In this figure, the effective energy is plotted on the right-hand axis (in the form $\sqrt{2E}$) and the value of R is plotted on the slanted central axis. The value of Vp is found by drawing a straight line from the appropriate point on the energy axis, through the value of R in the central axis, and onto the left-hand axis. The intercept point on the left-hand axis gives the flyer plate velocity.

Although the geometry used in this study was not flat, the results from this graph are likely to be a reasonable estimate of the flyer plate velocity.

TABLE I. - PROPERTIES OF EXPLOSIVES

Explosive	Density (kg/m^3)	E (kJ/kg)	Caloric Energy Density (kJ/kg)
Detasheet	1,470	3300	3400
Amatol	1,600	2000	4100
ANFO	800	203	3400

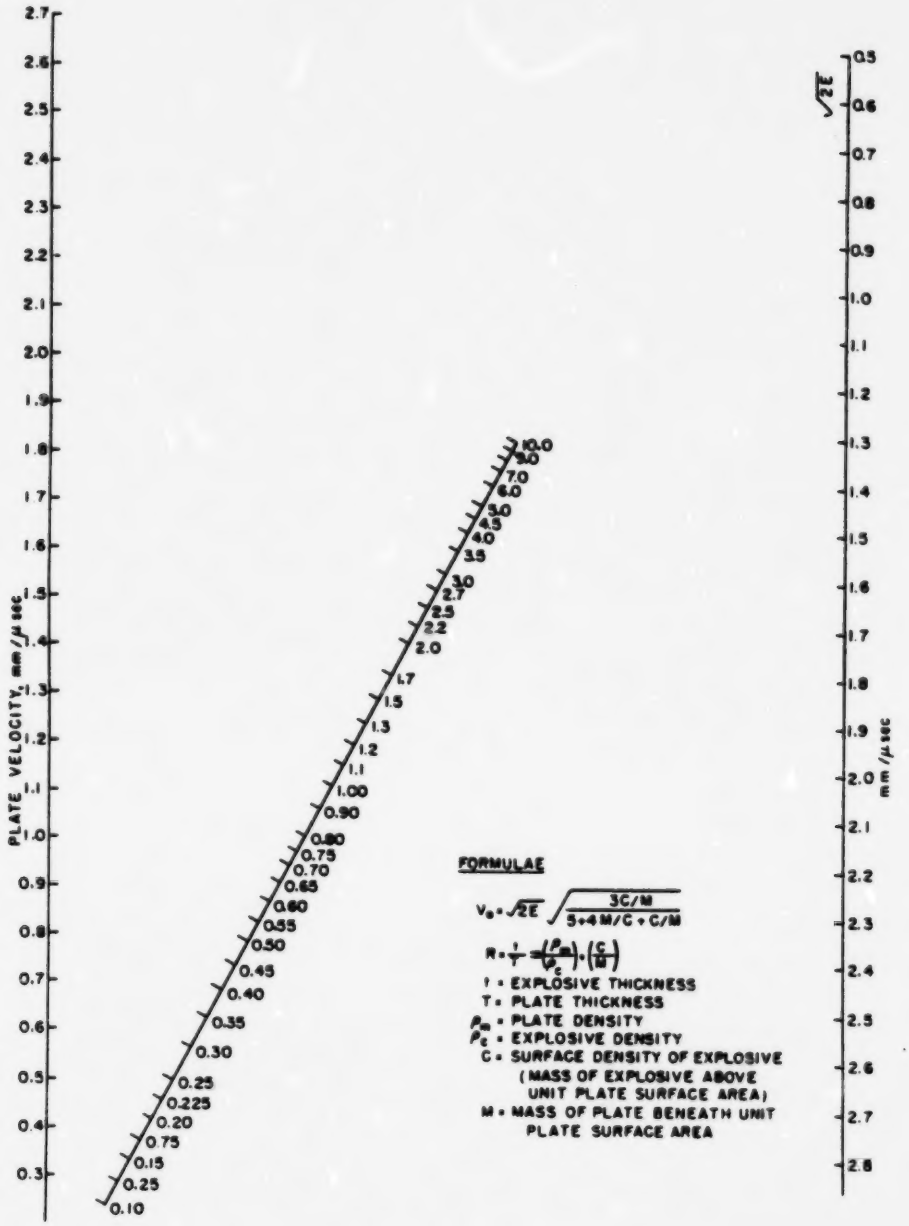
PLATE VELOCITY, mm/μsec
√2E
mm/μsec
FORMULAE
$V_o = \sqrt{2E}\sqrt{\frac{3C/M}{5+4M/C+C/M}}$
$R = \frac{t}{T} = \frac{(\rho_m)}{(\rho_c)} \cdot \left(\frac{C}{M}\right)$
t = EXPLOSIVE THICKNESS
T = PLATE THICKNESS
ρ_m = PLATE DENSITY
ρ_c = EXPLOSIVE DENSITY
C = SURFACE DENSITY OF EXPLOSIVE (MASS OF EXPLOSIVE ABOVE UNIT PLATE SURFACE AREA)
M = MASS OF PLATE BENEATH UNIT PLATE SURFACE AREA

Figure 1. Nomograph for the determination of flyer plate velocity (taken from [2]).

REFERENCES:

[1] B. Crossland, "Explosive Welding of Metals and Its Application", Clarendon Press, Oxford, 1985.

[2] M.A. Meyers, L.E. Murr, "Shock Waves and High-Strain-Rate Phenomena in Metals", Plenum Press, New York, 1981.

APPENDIX VI.

BRIEF DESCRIPTION OF PETRO-FORGE MACHINE

Final Report
Limpact Industries Limited

MODEL MK 11D-10K

Figure 1 shows the figures of the Petro-Forge machine at ORF and its working principle. The operation process is divided into four stages with (1) Injection stage, (2) Charging stage, (3) Working stroke stage and (4) Return stroke stage.

At the beginning of injection stage, the ram/piston assembly (A) Figure 1a, is held at the top of its stroke by low pressure air in the back pressure chamber (B) closing the combustion chamber porting by the seal (C), this being a cylindrical projection on the top face of the piston (A). The exhaust valve (D) is open and pressure in the combustion chamber (E) is atmospheric.

Upon pressing the firing button the fuel injection phase starts: the exhaust valve (D) is closed and the gaseous fuel is admitted into the combustion chamber (E) via the gas valve (F).

After closing the gas valve (F), the charge stage begins by admitting compressed air through the inlet valve (G). As soon as charging is completed, the inlet valve (G) is closed and the air/gas mixture is ignited by the spark plug (H). This results in a seven to eight-fold rise of the pressure in the combustion chamber (E).

As soon as the force due to the combustion pressure acting on the small area (I) on top of the seal (C) is sufficiently large to overcome the opposed force due to the low back pressure in the space (B) acting on the annular lower face of the piston, the piston (A) starts to move as the working stage begins.. As a result, the porting between the combustion chamber (E) and the cylinder is opened and the gases are permitted to expand to act over the whole piston area. This results in a large force surge acting on the piston/ram assembly which is accelerated downwards to impinge on the workpiece.

During the working stroke the back pressure in space (B) is intensified and consequently acts as a return spring as soon as the forming operation is completed, thus rapidly separating the dies as the return stroke stage. The return of the ram/piston assembly to its initial position is completed by the opening of the exhaust valve (D) which permits gases to leave through the duct (J). The cycle of operation is normally completed in one second.

Additional information on the machine performance is given on the following page.

	Nominal Maximum	Ultimate (Short Term)
Blow Energy	13.5 KJ (10,000 ft.lb.f)	27.0 KJ (20,000 ft.lb.f.)
Platen Velocity (Max.)	15 m/sec (50 ft/sec)	22 m/sec (70 ft/sec)
Stroke (Optimum)	250mm (10 in)	250mm (10 in)
Cycle Time	1.0 sec.	1.0 sec.
Adjustability of Blow Energy	8:1	16:1

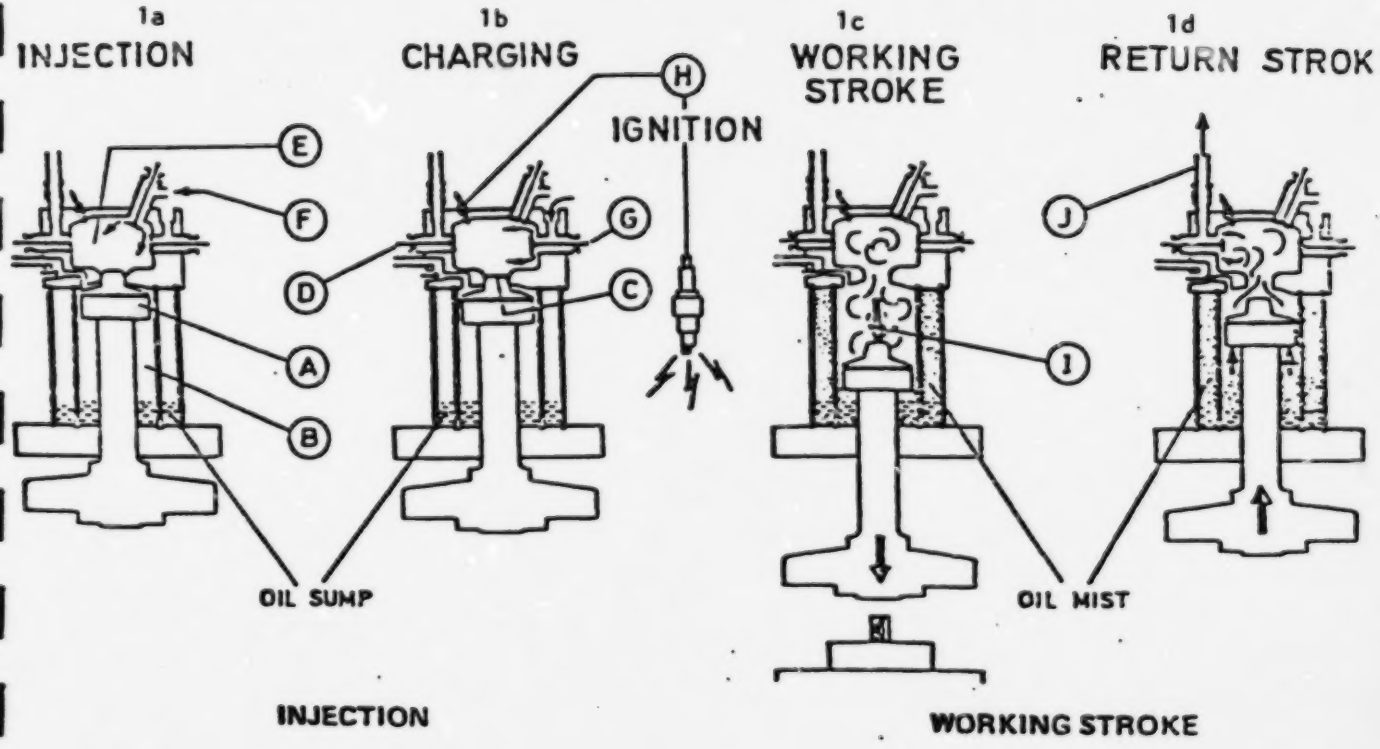

FIGURE 1. PETRO-FORGE MACHINE